Journal of Petroleum Science Research (JPSR) Volume 2 Issue 4, October 2013 www.jpsr.org
doi: 10.14355/jpsr.2013.0204.01

Aliphatic and Aromatic Biomarkers for Petroleum Hydrocarbon Investigation in Marine Sediment

Ines Zrafi[1], Leila Hizem[2], Houssem Chalghmi[2], Ahmed Ghrabi[1], Mahmoud Rouabhia[3]*, Dalila Saidane-Mosbahi[2]

[1]Centre de Recherches et des Technologies des Eaux (CERTE), Technopole Borj Cédria, BP 273, 8020 Soliman, Tunis, Tunisia
[2]Laboratoire d'Analyse, Traitement et Valorisation des Polluants de l'Environnement et des Produits, Faculté de Pharmacie de Monastir, Rue Avicenne 5000, Monastir, Tunisie
[3]*Groupe de recherche en écologie buccale, Faculté de médecine dentaire, 2420, rue de la Terrasse, Université Laval Québec (Québec), Canada G1V 0A6

[1]Zrafi_ines@yahoo.fr; [2]leila_hb@yahoo.fr; [3]houssem.chalghmi@yahoo.fr; [4]a.ghrabi@yahoo.fr; [5]mahmoud.Rouabhia@fmd.ulaval.ca; [6]dalila.saidane@fphm.rnu.tn

Abstract

Levels, composition profiles and sources of hydrocarbons were analyzed in surface marine sediment samples collected from Khniss Coast in Tunisia. It was found that the total Hydrocarbon (TH) concentrations ranged from 2280 μg/g to 7700 μg/g. The sedimentary non-aromatic hydrocarbon (NAH) and aromatic hydrocarbon (AH) concentrations ranged from 1020 to 2320 μg/g, and from 240 to 680 μg/g, respectively. The level of 17 polycyclic aromatic hydrocarbons (∑17PAHs) is equal to 14.59 ng/g. The PAH profiles showed that the ∑4–5-ring compounds were the major PAHs detected in the sampling sites. Characteristic ratios of Anth/(Anth+ Phe), and Flu/(Flu + Pyr) indicated that PAHs could originate from petrogenic and pyrolytic sources. Petroleum contamination associated with increased marine activity and high eutrophization statue in Khniss area which may have side-effects on the ecosystems and human safety; thus, it must be controlled.

Keywords

Marine Sediments; Petroleum Pollution; Aliphatics; Aromatics; PAH; Biomarkers

Introduction

Petroleum pollution has become a matter of serious environmental concern all over the world, because of its extensive use as energy source which has led to its widespread distribution in the biosphere (Diya'uddeen et al., 2011). Petroleum hydrocarbons (PHCs) come into the environment through accidents, spills or leaks, from industrial releases, or by products from commercial or domestic uses (Ou et al., 2004; Mille et al., 2007). PHCs are complex mixtures in both composition and molecular structure, mostly originating from crude oil. PHCs contain a wide range of chemical products such as gasoline, kerosene, fuel oil, heavy oil and lubrication oil. The total input of petroleum into the oceans through human activities, atmospheric fallout and natural seepage is estimated at 2.37 x 106 tones per year. Out of these, about 65% is discharged through household and industrial wastes, urban and river runoffs, oceanic dumping and atmospheric fallout; 26% is derived from discharge during transportation, dry docking, tanker accidents, and de-blasting (GESAMP, 1993). The fate of petroleum hydrocarbons in marine environment is subject to complex and interrelated physic-chemical processes that include evaporation, dissolution, photo-oxidation, microbial degradation, emulsification and sedimentation. These physical and chemical factors cause important modifications to the hydrocarbon compounds, which render them difficult to detect and to analyze (Wang and Fingas, 2005; Venkatachalapathy et al., 2011). The contamination of marine sediment by PHCs is widespread in coastal regions and represents a major concern for the potential detrimental consequences on ecosystems' health and provision. PHCs in water and air may reach the sediment by adsorption and deposition. Sediment becomes a primal carrier and environmental termination of PHCs (Michael et al., 2002). Sediment system can be considered as a major reservoir and sinks for marine pollutants because of its holding capacity for organic pollutants (Mille et al., 2007; Choi et al., 2011). It can also be a good indicator of environmental pollution (Baird et al., 2005;

Baudouin et al., 2007). Analyzing the composition of hydrocarbon compounds in marine sediments can provide much information about their sources and digenetic processes and reflect the extent of anthropogenic pressures on the environment (Hostettler et al., 1999; Medeiros et al., 2005; Zaghden et al., 2005). Therefore, non-aromatic hydrocarbons (NAHs), such as n-alkanes, unresolved complex mixture (UCM), and polycyclic aromatic hydrocarbons (PAHs) measured in sediment have been used to assess petroleum contamination in the marine environment (Beg et al., 2003; Ye et al., 2007; Da Silva et al., 2010; Maioli et al., 2010). The sources of these environmental geochemical markers are both natural and anthropogenic (Budzinski et al., 1997). Recent studies have examined the hydrocarbon status in Tunisian marine coasts (Louati et al., 2001; Zaghden et al., 2005; 2007; Trabelsi et al., 2005; Khedir-Ghenim et al., 2009) but to our knowledge, no information on hydrocarbon levels and origins in Khniss region is available. The Khniss area is situated at the Middle Eastern part of Tunisia. This coastal area is subject to important fishing activities and it receives several domestic wastes from the surrounding areas and especially the discharge of water from Wadi Khniss. Therefore, the identification and quantification of PHC compounds in this marine area will be of the utmost interest. The purposes of the present study were: i) to evaluate the hydrocarbons contamination levels from superficial marine sediment in the Khniss coastal area of Tunisia, ii) to obtain detailed information on the spatial distribution of the different fractions AH, NAH and PAH, iii) to determine the eventual sources for each fraction by using geochemical biomarkers.

Materials and Methods

Area of Study and Sampling

The area under study was located between 35°42′08.77′′N; 10°49′54.42′′E and 35°43′06.32′′N, 10°49′02.76′′E of Tunisia using the Global Positioning System (GPS). Sample collection occurred in 2008. Sediment samples were collected from superficial layer at four different sampling sites identified as Keniss Sediment-A (KSA), Keniss Sediment-B (KSB), Keniss Sediment-C (KSC) and Keniss Sediment-D (KSD). The coordinates of sampling sites are given in Table 1. The sediment samples were stored in pre-cleaned aluminum boxes at 4°C during transportation to the laboratory (with no exposure to light). The characteristics of the sediment samples were described in Table (1). At each site, three samples, separated by 3 m from each other, were taken. In our laboratory, the three sediment samples of the same site were mixed in order to increase the size of the samples and to recover the surface of sampling, manually homogenized, lyophilized, passed through a stainless steel sieve (200 and 100 μm) and finally stored at 4◦C until analysis. All the results were reported as dry weight.

Hydrocarbons Analysis

The total hydrocarbons (TH) present in 20 g of dry weight (dw) sediment were extracted in a Soxhlet apparatus with chloroform for 16 h. Recovery ranged from 97.4% to 98.9% for the n-eicosene. Following chloroform evaporation, the extract was fractionated into aliphatic and aromatic hydrocarbons by adsorption liquid chromatography using a column of alumina and silica-gel, and gradient solvents as eluent: n-hexane and 2:1 n-hexane/ chloroform for non-aromatic hydrocarbon (NAH) and aromatic hydrocarbon (AH) fractions, respectively. The NSO fraction (PF) was not eluted and calculated according to: NSO= TH – (NAH +AH). The total petroleum hydrocarbon (TPH) represents the sum of the NAH and AH fractions. Fractionation was performed in a silica micro-column (silica gel 60 of 63–200 μm). Prior to use, the silica was cleaned with chloroform, subjected to a one-hour wash at 50°C under magnetic agitation, and filtered through a glass fiber filter (type GF/A, 47 mm diam., 1.6 μm retention) (Whatman International, Kent, UK). The silica was then conditioned overnight at 110°C. Following solvent evaporation, the NAH and AH were weighed. The NAH were analyzed with a Hewlett-Packard 5890 gas chromatograph equipped with a temperature-controlled injector, a flame ionization detector (GC/ FID), and a capillary column HP5: 5%diphenyl, 95% dimethylpolisiloxane (25 m x 0.32 mm x 90.52 μm). The oven temperature program was as follow: 1 min at 80°C, from 80 to 280°C at 4°C/min and 10 min at 280°C. The injector and detector temperatures were 250°C and 280°C, respectively. The samples were solubilized in cyclohexane and 1 μl of this sample was injected following the addition of external standard (*n*-eicosene).

Aliphatic Hydrocarbon Analysis

Quantification of the total resolved (TR) hydrocarbon (n-alkanes) and unresolved complex mixtures (UCM) were calculated using the mean response factors of n-alkanes. Each hydrocarbon concentration was expressed as dry weight (dw). Recovery assays ranged from 94.50% to 98.12% for C18 nalkane and from 87.0% to 92.3% for a mixture of C10–C34 n-alkanes. Concentrations of individual n-alkanes (n-C12 to n-

C32), isoprenoids pristane and phytane, TR, UCM, and total aliphatic (TA) fraction (sum of identifiable aliphatic peaks + UCM) were calculated. The detection limit was determined at 0.001 μg/g for the C18 n-alkanes. Data of the TH, NAH, and AH concentrations are given as means ± SD (n = 3).

Aromatic Hydrocarbon Analysis

The AH were analyzed with a Hewlett-Packard 5890 gas chromatograph equipped with a temperature-controlled injector, a flame ionization detector (GC/FID), and a capillary column HP5: 5%diphenyl, 95%dimethylpolisiloxane (25 m x 0.32 mm x 90.52 μm) under the same temperature program and the same analytic conditions described for the NAH fraction (see section 1.2). The Gas Chromatography (GC) identification and quantification of PAHs was carried out as described by (Trablsi et al., 2005) based on the comparison with known standards injected under the same conditions. A certified standard reference (National Institute of Standards and Technology, USA) was used. Sixteen un-substituted PAHs have been listed by the US Environmental Protection Agency (EPA) as priority pollutants. The PAHs investigated in this study were: naphthalene (Naph), 1-methyl-naphthalene (1menaph), 1-ethyl-naphthalene (1enaph), ace-naphthylene (Ac), acenaphthene (Ace), 2,3,6-trimethyl-naphthalene (2,3,6- trimenaph), fluorene (Flu), phenanthrene (Phe), 2-methyl-phenanthrene (2-mephe), 1- methyl-phenanthrene (1-mephe), 3,6-dimethyl-phenanthrene (3,6-dimephe), fluoranthene (Fluo), pyrene (Pyr), 1-methyl-pyrene (1-mepyr), anthracene (Anth), chrysene (Chr), and perylene (Pery). When the peaks were not identified by GC, an analysis was carried out using a coupled GC/MS. The mass spectrometer was of type HP 9572 II (Agilent, California) (GC/MS) equipped with a Splitless injection system. The capillary column (30 m, 0.25 mm, 0.25 μm), the carrier gas was nitrogen. The GC conditions were the same as described (1.2 Hydrocarbon analysis) for CG/FID analysis. For the MS analysis, the electron ionization of 70 eV and linear scanning over the mass range 35–500 Da were used. Compound identification was based on individual mass spectra and GC retention times in comparison to the literature, library data, and standards. To ensure an appropriate quality of analyses, standards and blanks were analyzed under the same conditions as the samples. All analyses were done in triplicate.

Statistical Analyses

Data of the different fraction of hydrocarbon concentrations were statistically analyzed. For each fraction, standard errors were calculated between three repetitions analysis (n = 3). Results are expressed as mean SE (standard error). Comparisons among multiple groups of samples, for each site, were achieved by one-way ANOVA followed by Tukey's Multiple Comparison Test. Statistical significance was defined as $P < 0.05$.

TABLE 1 LOCATIONS AND CHARACTERISTICS OF SAMPLING SITES IN KHNISS COAST FROM TUNISIA

Site	Station code	Localization		Size of sediment	Type of bottom	Depth
KSA	KSA-1	35°43′06,32′′N	10°49′02,76′′E	Fine grained sand<100 μm	Sand without seagrass	0-15 cm
	KSA-2	35°43′02,79′′N	10°49′12,46′′E	Fine grained sand<100 μm	Sand without seagrass	0-15 cm
	KSA-3	35°43′01,18′′N	10°49′05,71′′E	Fine grained sand<100 μm	Sand without seagrass	0-15 cm
KSB	KSB-1	35°42′52,51′′N	10°49′18,36′′E	Fine grained sand<100 μm	Meadow of seagrasses	0-15 cm
	KSB-2	35°42′47,37′′N	10°49′21,32′′E	Fine grained sand<100 μm	Meadow of seagrasses	0-15 cm
	KSB-3	35°42′44,60′′N	10°49′23,02′′E	Fine grained sand<100 μm	Sand without seagrass	0-15 cm
KSC	KSC-1	35°42′34,87′′N	10°49′25,64′′E	Fine grained sand<100 μm	Sand without seagrass	0-15 cm
	KSC-2	35°42′31,45′′N	10°49′32,98′′E	Fine grained sand<100 μm	Sand without seagrass	0-15 cm
	KSC-3	35°42′28,06′′N	10°49′31,32′′E	Fine grained sand<100 μm	Sand without seagrass	0-15 cm
KSD	KSD-1	35°42′14,68′′N	10°49′37,95′′E	Fine grained sand<100 μm	Meadow of seagrasses	0-15 cm
	KSD-2	35°42′05,38′′N	10°49′47,71′′E	Fine grained sand<100 μm	Meadow of seagrasses	0-15 cm
	KSD-3	35°42′08,77′′N	10°49′54,42′′E	Fine grained sand<100 μm	Meadow of seagrasses	0-15 cm

KSA, KSB, KSC and KSD : sampling site.

TABLE 2 HYDROCARBON CONCENTRATIONS (μG/G ± SE DRY WEIGHT) IN MARINE SEDIMENTS FROM KHNISS COASTAL

Site reference	TH	NAH	%NAH	AH	%AH	NSO	%NSO	TPH	%TPH	TPH/NSO
KSA	4060±24.2	2260±20.3	55.6	240±9.1	5.9	1560±15.7	38.5	2500±11.9	61.5	1.6
KSB	7700±48.4	1650±12.8	21.2	340±11.4	4.4	5710±26.2	74.3	1990±10.8	25.7	0.34
KSC	2280±17.1	1020±14.2	44.7	330±8.4	14	930±19.7	41.3	1350±16.4	58.7	1.45
KSD	7050±21.1	2320±16.1	32.9	680±14.2	9.6	4050±21.4	57.4	3000±23.2	42.6	0.74

KSA, KSB, KSC and KSD: sampling site.

TH: Total hydrocarbons; NAH: Non aromatic hydrocarbons; AH: Aromatic hydrocarbons; NSO: Heavy compounds; TPH: Total petroleum hydrocarbons. These are expressed as μg/g dwt of sediment by using gravinemetry analyses.

Results and Discussion

Distribution of TH, NAH and AH in Sediment

The sediment samples from KSA, KSB, KSC and KSD were subjected to an organic analysis to determine the biogenic and anthropogenic hydrocarbon input in the region. Results of total hydrocarbons, non-aromatic hydrocarbon, aromatic hydrocarbon and total petroleum hydrocarbon were reported in Table 2. Results show high TH levels in all the sites of study, which may be due to anthropogenic, terrestrial and marine organic matter inputs. TH concentrations differed from one site to another. KSB and KSD registered the highest TH levels with 7700 ± 48.4 μg/g dw and 7050 ± 21.1 μg/g dw, respectively. These high levels could be due to the contribution of biogenic hydrocarbons in these sites as confirmed by the significant dominance of heavy fraction (NSO) in both KSB and KSD. Similar results were reported in the northern coast of Sfax-Tunisia (1127 μg/g and 5217 μg/g) (Louati et al., 2001). Total hydrocarbon levels in the Jarzouna Mediterranean coastal area ranged from 602 ± 7.638 μg/g dw to 1270 ± 2.176 lg/g dw (Khedir-Ghenim et al., 2009). These levels were higher than those found in the Gulf of Fos area of France (10.3–260.0 μg/g) (Mille et al., 2007). Biogenic hydrocarbons are generated either by biological processes or in the early stages of digenesis in recent marine sediments. Biological sources include land plants, phytoplankton, animals, bacteria, macroalgae, and microalgae (Wang et al., 2003). Furthermore, NAH and AH levels showed variations among the collection sites, with an average of 1020±14.2-2320±16.1 μg/g for NAH and 240±9.1-680±14.2 μg/g for AH (Table 2).

The highest NAH levels were found in KSA and KSD sampling sites, while the most elevated aromatic fraction level is associated to KSD site. NAH are predominant in the TPH fraction in each sediment sample. NAH percentages varied from 21.2% to 55.6%, while the aromatic percentages varied from 4.4% to 14 %. These percentages are comparable to those found in previous study (Zrafi-Nouira et al., 2008) in the Jarzouna region in Bizerte (Tunisia) confirming petroleum origin of hydrocarbons. The ratio of TPH fraction/heavy hydrocarbons (NSO) may indicate the origin of organic matter in sediment. KSB and KSD sites have a ratio TPH/NSO <1, which indicates biogenic origin of hydrocarbons (Table 3). On the other side, KSA and KSC have a ratio TPH/NSO >1, which confirms petroleum origin of hydrocarbons from these sites. KSA and KSC sediment hydrocarbons displayed typical characteristics of crude oil, as the TPHs were over 50%. Our results showed biogenic input in the KSB and KSD sites, and suggest petroleum origin in sediments from KSA and KSC. We also demonstrated that the total hydrocarbon levels in the Khniss Mediterranean coastal area ranged from 2280±17.1 μg/g dw to 7700±48.4 μg/g dw (Table 2). These levels were higher than those found in the northern coast of Sfax-Tunisia (1127-5217 μg/g) (Louati et al., 2001). Total hydrocarbon concentrations can be classified as relatively high by comparison with other coastal Mediterranean sediments (Grimlat et al., 1990; Le Dreau et al., 1981; Mille et al., 2007) and other coastal sediments (Massoud et al., 1998; Beg et al., 2003, Gao et al., 2008). The NAH levels recorded in all the sites are relatively high (Table 3) compared to those recorded in the area of Sfax (Elloumi et al., 2008), which vary from 26.7 to 127.8 μg/g and those recorded (Commendatore et al., 2004) in the Patagonia region in Argentina, ranging from 0.27 to 1304.7 μg/g. Levels of

TABLE 3 LEVELS OF NAH (μg/g DRY WEIGHT) IN THE TWO POLLUTED SITES (KSA AND KSC) FROM SEDIMENT OF KHNISS

	KSA (μg/g)	KSC (μg/g)
C9	4 .55 10^{-01}	4.55 10^{-01}
C10	1.15	1.15
C12	2.24 10^{-03}	2.24 10^{-03}
C13	8.94 10^{-05}	8.94 10^{-05}
C14	2.8 10^{-03}	2.80 10^{-03}
C15	2.99 10^{-03}	2.99 10^{-03}
C16	3.47 10^{-02}	3.47 10^{-02}
Pr	3.24 10^{-01}	3.24 10^{-01}
C17	1.18 10^{-01}	1.18 10^{-01}
Ph	3.00 10^{-01}	3.00 10^{-01}
C18	9.50 10^{-01}	9.50 10^{-01}
C19	1.37	1.37
C20	2.15	3.03 10^{-01}
C21	1.43	2.10 10^{-01}
C22	1.70	1.2
C23	1.18	2.63 10^{-01}
C24	1.99	4.21 10^{-01}
C25	2.96	2.49 10^{-01}
C26	4.36	2.91 10^{-01}
C27	4.79	4.63 10^{-01}
C28	3.9	5.20 10^{-02}
C29	3.39	7.41 10^{-02}
C30	2.09	7.59 10^{-02}
C31	1.37	1.37
C32	ND	ND
Σn-alcanes	36.08	9.69
UCM	142.12	65.43
ΣLMW	6.88	5.02
ΣHMW	29.2	4.67

KSA and KSD: sampling site. C1 to C32: n-alcanes fractioned with GC chromatography .These are expressed as μg/g dwt of sediment.

UCM: Unresolved Complex mixture, LMW: low molecular weight; HMW: high molecular weight; ND: not detected

NAH varying from 60.7 to 1356.3 μg/g in the Eastern Harbor of Alexandria in Egypt (Aboul-Kassim et al., 1995). AH concentrations determined in Khniss sediments are relatively high, compared with those established in the sediments of the Gulf of Fos in France ranging from 2.5 μg/g to 80 μg/g (Mille et al., 2007) and in the sediment of Santos coastal area in Brazil which varied between 0.08 and 42.39 μg/g (Nishigima et al., 2001).

Aliphatic Biomarkers and Origins in Polluted Sites

Aliphatic hydrocarbons and NAH are considered as important petroleum fractions present in the marine sediments. Their sources are either natural, from photosynthesis by marine biota inhabiting the surface waters, or anthropogenic, from land run-off, fallout, and/or industrial input (Aboul-Kassim et al., 1995). The aliphatic hydrocarbon fraction is composed of n-alkanes, branched alkanes, isoprenoids and cyclic compounds. Their analysis can be used to fingerprint spilled oils and provides additional information on the source of hydrocarbon contamination and the extent of degradation of the oil spill (Tolosa et al., 2004). Petroleum compounds are generally readily identified by their gas chromatogram traces. NAH analysis was also carried out for aliphatic petroleum biomarkers identification (Table 4). Obtained GC traces show regular distribution ranged from n-C9 to n-C31 alkanes with equivalent distribution pattern of both odd carbon-numbered alkanes and even-carbon-numbered alkanes. In fact, GC trace analysis showed unimodal n-alkane distribution at KSA which is a distribution with single mode indicating unique source of pollution whereas bimodal distribution was found in KSC. In this last case a mixture of two normal distributions with the same variance but different means are observed in the GC traces which demonstrate the presence of two different sources of petroleum pollution (gasoline, crude oil, diesel…). It is recognized from the literature that both unimodal and bimodal n-alkane distributions ranging from n-C15 to n-C32 are characteristic of petroleum origin (Yang et al., 2009). Bimodal distribution is observed for certain oil products. It also may be due to the superposition of two different types of petroleum product sources (Yang et al., 2009). This possibility is more probable for the KSA sediments, considering the nature of the petroleum products input during the sampling period and the nature of maritime activities in this region. Thus, this distribution is the result of a mixed origin of two types of petroleum products which the first is a refined product such as kerosene, fuel reactor and diesel products. These products are characterized by the presence of the n-alkanes range between n-C6 and n-C26 with a maximum of n-C26. This is the case of the chromatogram obtained from the KSA sediment NAH. The absence of n-C6 may be due to the evaporation which is generally observed for low molecular weight hydrocarbons (LMW). The presence of n-C9 and n-C10 in the chromatograms may also indicate a recent contamination with light distillated product such as diesel or gasoline (Yang et al., 2009). Both gasoline and diesel are also characterized with central UCM (Unresolved Complex Mixture) similar to that present in KSA sediment GC trace. UCM is an indicator of petroleum contamination and n-alkanes biodegradation (Mille et al., 2007). The chromatograms obtained from KSC sediment are characterized by the presence of n-alkanes ranged from n-C6 to n-C26 with developed UCM below the n-C26. UCM values in khniss samples (Table 3) are relatively higher than those recorded in the Bay of Marseille (11-230 mg/Kg sed. Dry weight) (France) (Asia et al., 2009), but relatively low compared to those found in sediment from Sfax region-Tunisia (Zaghden et al., 2005). An equivalent distribution pattern of both odd carbon-numbered alkanes and even carbon-numbered alkanes resulting in a carbon preference index (CPI) near the unit was also found in KSA and KSC sediments (Table 4). CPI values are suggested to be a useful indicator of the relative contribution of n-alkanes from fossil hydrocarbons and biogenic emissions, and several studies have confirmed oil CPI values to be around 1.0 (Zheng et al., 2005, Wang et al., 2003; Kalaitzoglou et al., 2004). Table 4 also presents the different ratios of Pr/Ph, Pr/C17 and Ph/C18 which are used to identify the anthropogenic origin when ≤1. At the same ∑LMW/∑HMW (when ≥1) and UCM/∑n-alkanes (when >2), confirm petroleum origin in KSA and KSC (Table 4). C17/C29, NAR and TAR were however, suggesting the biogenic contribution in KSA and KSC (Table 4). The nC17/C29 ratio indicates the relative presence of allochthonous and autochthonous hydrocarbons in the samples; this confirms the limited contribution of marine origin at KSA and their dominance at KSC. In fact n-C29 is abundant in land plants and n-C17 is dominant in marine organisms. The terrigenous/aquatic ratio (TAR), which reflects the long-chain n-alkane (n-C27 + n-C29 + n- C31) to short-chain n-alkane (n-C15 + n-C17 + n-C19), can be useful to confirm the importance of terrigenous and aquatic inputs (Bourbonniere et al., 1996). Biogenic sources of

TABLE 4 ALIPHATIC AND AROMATIC BIOMARKERS IN KSA AND KSC SEDIMENTS

	Aliphatic Biomarkers								
	UCM/∑n-alcanes	**CPI**	**Pr/Ph**	**Pr/C17**	**Ph/C18**	**C17/C29**	**NAR**	**TAR**	**∑LMW/∑HMW**
KSA	3.93	1	1.08	2.74	0.31	0.03	0.008	6.37	0.23
KSC	6.75	1.2	1.08	2.74	0.31	1.59	0.26	1.27	1.07
	Aromatic biomarkers								
	ΣMphe/Phe	**DMphe/Phe**	**Phe/Anth**	**Anth/Anth+Phe**	**Fluo/Pyr**	**Fluo/Fluo+Pyr**			
KSA	3.78	0.59	nd	0	0	0			
KSC	8.62	0.15	2.61	0.28	0.04	0.07			

UCM/∑n-alcanes : Unresolved Complex Mixture/sum of n-alcanes ; CPI : Carbon Preference Index ; Pr : Pristane ; Ph : Phytane ; NAR : Natural n-Alkane Ratio; TAR : Terrigenous/Aquatic Ratio ; ∑LMW/∑HMW : sum of n-alcanes of low molecular weight / sum of n-alcanes of high molecular weight. DMPhe: 3,6-dimethylphenanthrene ; Fluo: Fluoranthene ;∑Mphe: 1-methylphenanthrene+2-methylphenanthrene ; Pyr: Pyrene ; Phe: Phenanthrene ; nd: non-determine ; Anth: Anthracene.

hydrocarbon come from both inputs. The TAR ratio was higher than 1 at KSA, but was near the unit in the KSC site (Table 4). The natural n-alkane ratio (NAR) is used to estimate the proportions of natural and petroleum n-alkanes (Mille et al., 2007). The values of NAR ratio is close to 0 for petroleum hydrocarbon and close to 1 for terrestrial or marine plants. In our study, no value close to 1 was registered at each of the investigated sites (Table 4). NAH analysis therefore shows that the limited biogenic source contribution is explained by the mix of terrestrial input and marine hydrocarbons. A fishing site is in fact located near several maritime activities. Observing the n-alkane distribution and performing a marker analysis enabled us to render a hypothesis of petroleum source contribution with limited biogenic contribution in both KSA and KSC sediments.

PAHs Distribution in Polluted Sediments

Aromatic hydrocarbons were analyzed to reveal the presence of PAHs contamination relative to pyrolytic or petrogenic origins in Khniss sediments. Table 5 presents the total PAHs (Σ17 PAHs) and individual PAH concentrations. Results show that Σ17PAHs concentrations vary from 6.95 ng/g in KSC to 14.59 ng/g in KSA. The Khniss coastal area is home to many small industries and maritime activities, which may explain the observable difference between the concentrations in the sediments. In fact this region is subject to hydrocarbon pollution by sewage, industrial and aquacultural waste, and other human activities. An understanding of the local and global extent and severity of marine environment contamination by fossil fuel hydrocarbons from various sources requires measuring the compounds of interest and comparing them in different regions. The total PAHs concentration we measured in the Khniss coastal region indicates that the sediment contamination is important, and comparable to that found in other locations around the world (Table 6). National comparison revealed, elevated PAH concentrations in the lagoon of Bizerte (83.3 ng/g to 447) (Trabelsi et al., 2005) and in the coastal area of Sfax and Kerkennah (113 ng/g to 10720 ng/g) (Zaghden et al., 2007). This comparison also showed that the Khniss region showed lower sedimentary concentrations of PAHs compared with those found in the sediment of Vendres harbor in France (145 to 6940 ng/g (Baumard et al., 1998), and Haihe River in Chine (775 to 255372 ng/g) (Bin et al., 2007). The distribution of the individual PAH in KSA and KSC is reported in Table 5. In sediment from KSA

TABLE 5 PAH LEVELS (ng/g DRY WEIGHT) IN KSA AND KSC SEDIMENTS

	KSA ng/g	**KSC ng/g**
Naph	$3.47\ 10^{-1}$	$1.14\ 10^{-1}$
1menaph	-	$2.10\ 10^{-1}$
1enaph	-	$1.98\ 10^{-1}$
Ac	-	$2.23\ 10^{-1}$
Ace	1.62	$1.82\ 10^{-1}$
2,3,6 trimenaph	-	$3.86\ 10^{-2}$
Flu	$5.03\ 10^{-2}$	$7.19\ 10^{-3}$
Phe	$4.31\ 10^{-3}$	$8.70\ 10^{-2}$
Anth	-	$3.34\ 10^{-2}$
2-mephe	$1.63\ 10^{-2}$	$8.54\ 10^{-2}$
1-mephe	-	$6.65\ 10^{-1}$
3,6-dimephe	$2.54\ 10^{-3}$	$1.28\ 10^{-2}$
Fluo	-	$7.55\ 10^{-2}$
Pyr	$1.80\ 10^{-3}$	1.93
1-mepyr	$3.29\ 10^{-3}$	$5.16\ 10^{-1}$
Chr	12.35	1.62
Pery	$1.83\ 10^{-1}$	$9.52\ 10^{-1}$
∑ *PAH*	14.59	6.95
∑ *2-3 rings*	2.05	1.86
∑ *4-5 rings*	12.5	5.1

Abbreviations: Naphthalene (Naph), 1methyl-naphthalene (1menaph), 1ethyl-naphthalene (1enaph), acenaphthylene (Ac), acenaphthene (Ace), 2,3,6 trimethyl-naphthalene (2,3,6 trimenaph), fluorene (Flu), phenanthrene (Phe), 2-methyl-phenanthrene (2-mephe), 1-methyl phenanthrene (1-mephe), 3.6-dimethyl-phenanthrene (3,6-dimephe), fluoranthene (Fluo), pyrene (Pyr), 1-methyl-pyrene (1-mepyr), anthracene (Anth), chrysene (Chr), and perylene (Pery): these are expressed as ng/g of sediment by using GC analyses.

TABLE 6 COMPARISON OF SEDIMENT PAH CONCENTRATION (ng/g DRY WEIGHT) OF KHENISS COASTAL WITH THOSE IN OTHERS REGIONS

Sediments	PAHs (ng/g)	Refernces
Khniss coast, Tunisia	6.95-14.59	This study
Jarzouna coast, Tunisia	916.4-4541.1	Zrafi-Nouira et al 2008
Lagune of Bizerte, Tunisia	83.3-447	Trabelsi et al 2005
Kerkennah-Sfax coast, Tunisia	113-10720	Zaghden et al 2005
Vendres harbour, France	145-6940	Baumard et al 1998
Baltic Sea	720-1900	Witt et al 1995
Porto Torres harbour, Sardaigne, Italie	70-1210	De luca et al 2004
Baie Kyeonggi, Corée	9.1-1400	Kim et al 1999
Malaisie	4-924	Zakaria et al 2002
Haihe River, Chine	775-255372	Bin et al 2007
Deep Baie, Chine	353.8	Qiu et al 2009

site, we noticed the absence of 1-methyl-Naphthalene, 1-ethyl-Naphthalene, Acenaphthene, 2,3,6-trimethyl-Naphthalene, Anthracene, 1-methyl phenanthrene and Fluoranthene and the relative abundance of Naphthalene, Acenaphthene, Fluorene, Chrysene and Perylene. In KSC sediment; results show the presence of all target PAHs with the abundance of Fluorene, Pyrene, 1-methyl Pyrene, Chrysene and Perylene. Chrysene is the most important representative toxic PAH, in KSC (Table 5). High concentrations of chrysene can be associated with the weathering effect in crude oil's chemical composition change. In addition, high concentrations of Chrysene which is considered as a "conservative" PAH due to its resistance to weathering and bacterial degradation (Wang et al., 2003); indicates petroleum contamination input in this site. Higher concentrations of perylene could however, result from terrigenous precursors whose diagenetic degradation could lead to the formation of perylene and indicates biogenic contribution (Venkatesan et al., 1988).

PAH Compound Profiles and Origins

The analysis of the Low Molecular Weight PAHs (LMW-PAHs) and High Molecular Weight PAHs (HMW-PAHs) were useful in the characterization of petroleum pollution and an interpretational advantage in fingerprinting sources of spilled oils and for providing additional diagnostic information. Analysis of individual PAH characteristics from Khniss sediments showed the predominance of HMW-PAH (4-5-ring PAH). Petrogenic source contains relatively higher concentrations of individual LMW-PAH (2-3-ring PAH) compounds (Tolosa et al., 1996), while a high-molecular weight parent PAHs dominance is a typical characteristic of a pyrolytic source: combustion origin (Budzinski et al., 1997). HMW-PAHs have been recognized as directly carcinogenic and evidence suggests that the environmental persistence and genotoxicity of PAHs increase as the molecular size of the PAHs increases up to four or five fused benzene rings (Cerniglia et al., 1992). On the other hand dominance of the HMW-PAHs can be due to their strongly adsorbed by sediments whereas low molecular weight PAHs are subject to several degradation (Wang et al., 2003; Jones et al., 1986). Pyrolytic (fossil fuel combustion and vegetation fires) and petrogenic (oil spill and petroleum products inputs) are the primary sources of PAHs found in coastal marine sediments. Our results are comparable to those showing predominance of high molecular weight in the surface sediment of Jiaozhou Bay in China (Wang et al., 2006). The identification of the pollution origin is also based on the identification of compounds with specific sources. In fact, the presence of Fluoranthene (Fluo) and Pyrene (Pyr) indicates the importance of pyrolytic inputs since these compounds are considered as products formed from the condensation of aromatic compounds of low molecular weight at high temperature (Zeng et al., 1997; Wang et al., 1999). Chrysene is considered as a preserved biomarker of PAHs and it was selected to be a good marker of petroleum compounds because of its resistance to abiotic factors and bacterial degradation (Wang et al., 2003). Chrysene showed relatively high concentration in KSA site sediment, reflecting a petrogenic contamination. In addition, some diagnostic ratios (Fluo/Pyr, Phe/Anth, Fluo/Fluo+Pyr, Anth/Anth and ΣMphe+Phe/Phe) were used to distinguish between petrogenic and pyrolytic PAHs (Bin et al., 2007) (Table 4). Phe/Anth ratio under 3 indicates pyrolytic origin and it indicates petrogenic origin when it is over 3 (Ke et al., 2002; Tolosa et al., 2009).

On the other hand, a ratio (Anth/Anth+Phe) <0.1 indicates a petrogenic source, while this ratio indicates a combustion source when it is greater than 0.1. The ratio of Fluo/Pyr <1 is characteristic of a petrogenic source and the ratio Fluo/Pyr >1 characterizes a pyrolytic source. The ratio (Fluo /Pyr + Fluo) differentiates between petroleum, wood, coal and

plants combustion. When Fluo/Pyr+Fluo <0.5, it is generally associated with petrogenic source as a characteristic of fuel combustion (gasoline, diesel and crude oil), while when this ratio exceeds 0.5 it characterized pyrolytic sources (kerosene, wood, terrestrial plants and coal combustion) (Yunker et al., 2002; Mille et al., 2007). Phe/Anth and Anth/Anth+Phe ratios indicate that PAHs present in KSC sediment derived from pyrolytic sources. This pyrolytic origin is however not exclusive since the values of Fluo/Pyr and Fluo/Pyr+Fluo ratios show the contribution of oil sources (lubricating oils) in KSA and KSC sediment indicating mixed origin of PAHs.

Conclusion

This work represents the first detailed study on the distribution of hydrocarbons in the Khniss Tunisian-Coast sediments, their characterization and their possible sources. It extends our understanding of the current TH, NAH, AH and PAHs contamination status in this Mediterranean area. Hydrocarbons concentrations are relatively high compared to sedimentary concentrations along the Mediterranean coasts. Analysis of aliphatic, aromatic and PAHs hydrocarbons suggests an anthropogenic contamination in KSA and KSC sites, while hydrocarbons in KSB and KSD sites were characterized by biogenic sources. Hydrocarbon sources may therefore be related to wastewater and wadi Khniss discharges, harbor activities, fishing industries, atmospheric emission and extensive maritime traffic.

ACKNOWLEDGEMENTS

This study was partly supported by grants from the Ministry of Higher Education, Scientific Research and Biotechnology of Tunisia, and the University of Monastir.

REFERENCES

Aboul-Kassim TAT, Simoneit BRT "Petroleum hydrocarbon fingerprinting and sediment transport assessed by molecular biomarker and multivariate statistical analyses in the eastern harbour of Alexandria, Egypt" Mar. Pollut. Bull. 30: 63-73. (1995)

Asia L, Mazouz S, Guiliano M, Doumenq P, Mille G "Occurrence and distribution of hydrocarbons in surface sediments from Marseille Bay (France)." Mar. Pollut. Bull. 58: 424-455. (2009).

Baird WM, Hooven LA, Mahadevan B "Carcinogenic polycyclic aromatic hydrocarbon DNA adducts and mechanism of action". Environ. Mol. Mutagen. 45: 106-114. (2005).

Baudouin C, Charveron M, Tarroux R, Gall Y " Environmental pollutants and skin cancer." Cell Biol. Toxicol. 18: 341-348. (2007).

Baumard P, Budzinski H, Michon Q, Garrigues P, Burgeot T, Bellocq J" Origin and bioavailability of PAHs in the Mediterranean sea from mussel and sediment records. Estuary Coast. Shelf. S. 47(1): 77-90. (1998).

Beg M U, Saeed T, Al-Muzaini S, Beg KR, Al-Bahloul M "Distribution of petroleum hydrocarbon in sediment from coastal area receiving industrial effluents in Kuwait." Ecotoxicol. Environ. Saf. 54(1): 47-55. (2003).

Bin J, Hai-Long Z, Guo-Qiang H, Hui D, Xin-Gang L, Hong Tu S, Rui L "Characterization and distribution of polycuclic aromatic hydrocarbon in sediments of Haihe River, Tianjin, China." J. Environ. Sci. 19: 306-311. (2007).

Bourbonniere RA, Meyers PA "Sedimentary geolipid records of historical changes in the watersheds and productivities f lakes Ontario and Erie."Limnol. Oceanogr. 41: 352-359. (1996).

Budzinski H, Jones I, Bellocq J, Piérard C, Garrigues P "Evaluation of sediment contamination by polycyclic aromatic hydrocarbons in the Gironde estuary". Mar. Chem. 58: 85-97. (1997).

Cerniglia CE "Biodegradation of polycyclic aromatic hydrocarbons". Biodegradation. 3: 351-368. (1992).

Choi HG, Moon HB, Choi M, Yu J "Monitoring of organic contaminants in sediments from the Korean coast: Spatial distribution and temporal trends (2001–2007)." Mar. Pollut. Bull. 62(6):1352-61. (2011).

Commendatore MG, Esteves JL "Natural and anthropogenic hydrocarbons in sediments from the Chubut River (Patagonia, Argentina)." Mar. Pollut. Bull. 48: 910-918. (2004).

Da Silva DAM, Bícego MC "Polycyclic aromatic hydrocarbons and petroleum biomarkers in São Sebastião Channel, Brazil: Assessment of petroleum contamination." Marine. Environ. Res. 69: 277-286. (2010).

De luca et al. De Luca, G., Furesi, A., Leardi, R., Micera, G., Panzanelli, A., Piu, P.C., Sanna, G. "Polycyclic aromatic

hydrocarbons assessment in the sediments of the Porto Torres harbor (Northern Sardinia, Italy)" Mar.Chem. 86: 15–32. (2004).

Diya'uddeen BH, Ashri Wan Daud WM, Abdul Aziz AR. "Treatment technologies for petroleum refinery effluents": A review. Process. Saf. Environ. 89: 95-105. (2011).

Elloumi J, Guermazi W, Ayadi H, Bouain Aleya L "Detection of Water and Sediment pollution of An Arid Saltern (Sfax, Tunisia) by Coupling the Distribution of Microorganisms With Hydrocarbons." Water Air Soil Poll. 187: 157-171. (2008).

Gao X, Chen S "Petroleum pollution in surface sediments of Daya Bay, South China, revealed by chemical fingerprinting of aliphatic and alicyclic hydrocarbons." Estuar. Coast. Shelf. S. 80: 95-102. (2008).

GESAMP "Impact of Oil and Related Chemicals and Wastes on the Marine Environment." In: Report and Studies, GESAMP, vol. 50, 180 pp. (1993).

Grimlat JO, Albaiges J "Characterization of the depositional environments of the Ebro Delta (Western Mediterranean) by the study of sedimentary lipid markers." Mar. Geol. 95: 207-224. (1990).

Hostettler FD, Pereira WE, Kvenvolden KA, Van Green A, Luoma SN, Fuller CC, Anima R A "Record of hydrocarbon input to San Francisco Bay as traced by biomarker profiles in surface sediment and sediment core." Mar. Chem. 64: 115-127. (1999).

Jones DM, Rowland SJ, Douglas AG, Howells S "An examination of the fate of Niggerian crude oil in surface sediments of the Humber estuary by gas chromatography and gas chromatographymass spectrometry." Int. J. Environ. An. Ch. 24: 227-247. (1986).

Kalaitzoglou M, Terzi E, Samara C "Patterns and sources of particlephase aliphatic and polycyclic aromatic hydrocarbons in urban and rural sites of western Greece." Atmos. Environ. 38: 2545-2560. (2004).

Ke L, Wong TWY, Wong YS, Tam NFY "Fate of polycyclic aromatic hydrocarbons (PAH) contamination in mangrove swamp in Hong Kong following an oil spill." Mar. Pollut. Bull. 45: 339-347. (2002).

Khedir-Ghenim Z, Zrafi-Nouira I, Bahri R, Belayouni H, Hammami M, Rouabhia M, Saidane-Mosbahi D "Identification and distribution of petroleum hydrocarbons in sediments, seawater and Ruditapes decussatus collected from a Mediterranean Sea site." Int. J. of Water. 5: 35-50. (2009).

Kim GB, Maruya KA, Lee RF, Lee JH, Koh CH, Tanabe S "Distribution and sources of polycyclic aromatic hydrocarbons in sediments from Kyeonggi Bay, Korea". Mar Pollu Bull 38: 7–15. (1999).

Le Dreau Y, Jacquot F, Doumenq P, Guiliano M, Bertan JC, Mille G " Hydrocarbon balance of a site which had been highly and chronically contaminated by petroleum wastes of refinery (from 1956 to 1992)." Mar. Pollut. Bull. 34: 456-468. (1981).

Louati A, Elleuch B, Kallel M, Saliot A, Dagaut J, Oudot J "Hydrocarbon Contamination of Coastal Sediments from the Sfax Area (Tunisia), Mediterranean Sea." Mar. Pollut. Bull.42: 445-452. (2001).

Maioli OLG, Rodrigues KC, Knoppers BA, Azevedo DA "Pollution source evaluation using petroleum and aliphatic hydrocarbons in surface sediments from two Brazilian estuarine systems." Org. Geochem. 41: 966-970. (2010).

Massoud MS, Al-Abdali F, Al-Ghadban AN (1998). The status of oil pollution in the Arabian Gulf by the end of 1993. Environ. Int. 24: 11-22.

Medeiros PM, Bicego MC, Castelao RM, Rosso CD, Fillmann G, Zamboni AJ "Natural and anthropogenic hydrocarbon inputs to sediments of Patos Lagoon Estuary, Brazil." Environ. Int. 31: 77-87. (2005).

Michael S, Mclachlan GC, Frank W "The influence of vertical sorbed phase transport on the fate of organic chemicals in surface soils." Environ. Sci. Technol. 36: 4860-4867. (2002).

Mille G, Asia L, Guiliano M, Malleret L, Doumenq P "Hydrocarbons in coastal sediments from the Mediterranean sea (Gulf of Fos area, France)." Mar. Pollut. Bull. 54: 566-575. (2007).

Nishigima FN, Weber RR, Bícego MC "Aliphatic and Aromatic Hydrocarbons in Sediments of Santos and Cananéia, SP, Brazil." Mar. Pollut. Bull. 42: 1064-1072. (2001).

Ou SM, Zheng JH, Zheng JS, Richardson BJ, Lam PKS "Petroleum hydrocarbons and polycyclic aromatic

hydrocarbons in the surficial sediments of Xiamen Harbour and Yuan Dan Lake, China." Chemosphere. 56: 107-112. (2004).

Qiu, Y. W., Zhang, G., Liu, G. Q., Guo, L. L., Li, X. D., & Wai, O. (2009). Polycyclic aromatic hydrocarbons (PAHs) in the water column and sediment core of Deep Bay, South China. Estuarine, Coastal and Shelf Science, 83, 60–66. (2009).

Tolosa I, De Mora S, Sheikholeslami MR, Villeneuve JP, Bartocci J, Cattini C. "Aliphatic and aromatic hydrocarbons in coastal caspian Sea". Mar. Pollut. Bull.48: 44-60. (2004).

Tolosa JM, Bayona YJ, Albaigés GS "Aliphatic and polycyclic aromatic hydrocarbons and sulphur/oxygen derivatives in north western Mediterranean sediments: spatial and temporal variability fluxes and budgets." Environ. Sci. Technol. 30: 2495-2503. (1996).

Trabelsi S, Driss MR "Polycyclic aromatic hydrocarbons in superficial coastal sediments from Bizerte Lagoon, Tunisia." Mar. Pollut. Bull. 50: 344-359. (2005).

Venkatachalapathy R, Veerasingam S, Basavaiah N, Ramkumar T, Deenadayalan K "Environmental magnetic and petroleum hydrocarbons records in sediment cores from the north east coast of Tamilnadu, Bay of Bengal, India." Mar. Pollut. Bull. 62: 681-690. (2011).

Venkatesan MI "Organic Geochemistry of marine sediments in Antarctic region: Marine lipids in McMurdo sound." Org Geochem. 12: 13-27. (1988).

Wang XC, Sun S, Ma HQ, Liu Y "Sources and distribution of aliphatic and polyaromatic hydrocarbons in sediments of Jiaozhou Bay, Qingdao, China." Mar. Pollut. Bull. 52: 129-138. (2006).

Wang Z, Fingas M, Page DS "Oil spill identification. J. Chromatogr. A. 843: 369- 411. (1999).

Wang Z, Fingas MF "Development of oil hydrocarbon fingerprinting and identification techniques." Mar. Pollut. Bull. 47: 423-452. (2003).

Witt,G "Polycyclic aromatic hydrocarbons in water and sediment of the Baltic Sea." Mar. Pollut. Bull. 31: 237–248. (1995).

Yang C, Wang Z, Hollebone BP, Brown CE, Landriault M "Characteristics of bicyclic sesquiterpanes in crude oils and petroleum products." J. Chromatogr. A. 1216: 1174-1191. (2009).

Ye B, Zhang Z, Mao T "Petroleum hydrocarbon in surficial sediment from rivers and canals in Tianjin, China. Chemosphere. 68: 140-149. (2007).

Yunker MB, Macdonald RW, Vingarzan R, Mitchell RH, Goyette D, Sylvestre S "PAHs in the Fraser River basin: a critical appraisal of PAH ratios as indicators of PAH source and composition." Org. Geochem. 33: 489-515. (2002).

Zaghden H, Kallel M, Elleuch B, Oudot J, Saliot A "Sources and distribution of aliphatic and polyaromatic hydrocarbons in sediments of Sfax, Tunisia, Mediterranean Sea." Mar. Chem. 105: 70-89. (2007).

Zaghden H, Kallel M, Louati A, Elleuch B, Oudot J, Saliot A "Hydrocarbons in surface sediments from the Sfax coastal zone, (Tunisia) Mediterranean Sea. Mar. Pollut. Bull. 50: 1287-1294. (2005).

Zakaria M P, Takada H, Tsutsumi S "Distribution of polycyclic aromatic hydrocarbons (PAHs) in rivers and estuaries in Malaysia: a widespread input of petrogenic PAHs". Environ Sci Technol, 36(9): 1907–1918. (2002).

Zeng EY, Vista CL "Organic pollutants in the coastal marine environment off San Diego, California. I. Source identification and assessment by compositional indices of polycyclic aromatic hydrocarbons. Environ. Toxicol. Chem. 16: 179-188. (1997).

Zheng M, Fang M, Wang F, To KL "Characterization of the solvent extractable organic compounds in PM2.5 aerosols in Hong Kong. Atmos. Environ. 34: 2691-2702. (2000).

Zrafi-Nouira I, Khedir-Ghenim Z, Zrafi F, Bahri R, Cheraief I, Rouabhia M, Saidane Mosbahi D "Hydrocarbon pollution in the sediment from the Jarzouna-Bizerte coastal area of Tunisia (Mediterranean Sea)." Bull Environ Contam Toxicol. 80: 566-572. (2008).

Zrafi-Nouira Ines; Zouhour Khedir-Ghenim; Raouf Bahri; Imed Cheraeif; Mahmoud Rouabhia; Dalila Saidane-Mosbahi "Hydrocarbons in Seawater and Interstitial Water of Jarzouna-Bizerte Coastal of Tunisia (Mediterranean Sea): Petroleum origin investigation around refinery rejection place". Water Air and Soil Pollution. Vol. 202 No.1: 19-31. (2009).

Ines Zrafi is a PhD degree researcher with the «Research and water technology center (CERTE), Technopole Borj

Cédria». Her research project is dedicated to investigate the presence, distribution and side effects of petroleum hydrocarbon.

Leila Hizem is a student preparing her Master under the supervision of Dr. Saidane Mosbahi.

Houssem Chalghmi is a student preparing her PhD degree under the supervision of Dr. Saidane Mosbahi**.** He is working on petroleum hydrocarbon in the North of Tunisia.

Ahmed Ghrabi is a Professor and researcher with the «Research and water technology center (CERTE), Technopole Borj Cédria». He is involved in teaching and in research related to environmental sciences, in general.

Dalila Saidane-Mosbahi is a Professor with the faculty of pharmacy, University of Monastir, Tunisia. She is involved in teaching and in research related to the impact of the pollutants on the human physiology, in general.

Mahmoud Rouabhia is a Professor and researcher with the Faculty of Dentistry of Laval University, Quebec, Canada. He is very active in cell biology, microbiology, immunology and tissue engineering. His research program involves the study of cellular and molecular mechanisms in promising specialties such as oral research, as well as basic and applied biotechnology to the environment and health. He already published over 100 publications in well-known scientific journals.

doi: 10.14355/jpsr.2013.0204.02

Corrosion Study of Pipeline Steel Weld Immersed in Sour Solution

R. Galvan-Martinez [*1], M. Salazar[2], R. Orozco-Cruz[1], M.A. Morales-Cabrera[3], A. Contreras[2]

[1]Anticorrosion group, Institute of Engineering, University of Veracruz, Boca del Río, Veracruz, Mexico.
[2]Mexican Petroleum Institute, Pipeline Integrity Program, Distrito Federal, México.
[3]Chemical Engineering Department, University of Veracruz, Poza Rica-Tuxpan, Veracruz, México.
[*1]rigalvan@uv.mx; salazarm@imp.mx; rorozco@uv.mx; migmorales@uv.mx; acontrer@imp.mx

Abstract

This work presents an electrochemical study of API X52 pipeline steel weld immersed in NACE solution saturated with hydrogen sulphide (H_2S). The electrochemical techniques, polarization curves and linear polarization resistance are used in the corrosion test of the steel weld samples with the focus on the three different zones of the weldment, heat affected zone (HAZ), weld bead (WB) and base metal (BM). In addition, a brief analysis was made in order to identify the corrosion product film. It was found that the increment of temperature and H_2S dissolved in the NACE solution increase the corrosion rate (CR) of the three different zones. HAZ was significantly affected by the corrosion test and the phases mackinawite, troilite and pyrrhotite were identified in the film of corrosion products.

Keywords

Polarization Curves; LPR; X52 Pipeline Steel; H_2S

Introduction

For the majority of steels used in construction, most welding processes are acceptable from a corrosion point of view; provided that the welded joint had been made in a proper manner and the correct filler materials had been chosen (Wranglen, 1985). The failures of steel welded have been attributed to corrosion of the selective zones of the weld. This corrosion that found in fusion zone and electrical resistance welded, occurs in several environments, and is not confined to one region of the weldments (Loto, 1989). During the welding thermal cycle, a relatively narrow region of the material is subjected to a wide range of peak temperatures and cooling rates, resulting in a variety of microstructures and changes in properties of the affected area. Dominant mechanisms influencing the corrosion behaviour of the weld, should be attributed to the the formation of microstructures susceptible to corrosion and the redistribution of sulphides during the weld thermal cycle (Olsen, 1997). In addition to welding, the "sour environment" can produce failures in the structures and pipeline steel of the oil and chemical industries. H_2S has been associated to damages by corrosion and stress corrosion cracking induced by sulphides or hydrogen (Cayard, 1997; Cheng, 1998; Huang, 1996). The increment of temperature and/or pressure can increase the aggressiveness of H_2S solution for the carbon steel. Steel corrosion in solutions containing H_2S can be represented according to following reactions (Ewing, 1955; Galván-Martínez, 2004,2005):

$$Fe + H_2S_{aq} \Rightarrow FeS + H_2 \quad (1)$$

Most corrosion studies on API X52 steel in environments containing H_2S or sulphide ions put the emphasis on the use of the electrochemical techniques on the study of multiples factors that can affect the corrosion behaviour, such as H_2S concentrations (Perdomo, 2002), corrosion inhibitors (Vásquez, 2003; Romero, 2004), hydrodynamic conditions (Galván-Martínez, 2004,2005), microorganisms (Galvan-Martinez, 2005; Borgne, 2007) and mechanical stresses (Li, 2006; Lu,2006). Nevertheless, little work has addressed the corrosion study of the X52 steel weld in these environments. This work presents the electrochemical results obtained during the corrosion of the weldment of X52 pipeline steel sample focused on the three different weld zones.

Experimental Procedure

TABLE 1 NACE BRINE COMPOSITION

Chemical reagent	Weight (g/l)
calcium chloride dihydrate	4.48
magnesium chloride sixhydrate	2.06
sodium chloride	106.58

An aqueous NACE brine solution was used as test environment. Table 1 shows the reagents that constitute the composition of this brine. All the tests were carried out at two different temperatures, 25°C and 50°C, atmospheric pressure and static conditions. In order to remove oxygen from the test solution, N_2 gas was bubbled into the test solution for a period of 30 minutes, prior to the implementation of the test. After oxygen removal, H_2S gas was bubbled into the test

solution until saturation was reached. The measured saturation pH was 3.5. In Table 2, it is possible to observe the chemical composition of the API X52 steel.

TABLE 2. CHEMICAL COMPOSITION OF THE API X52 STEEL

C	Mn	Si	P	S	Cu	Cr
0.08	1.05	0.26	0.019	0.003	0.019	0.02
Ni	**Nb**	**V**	**Ti**	**Al**	**Fe**	
0.02	0.041	0.054	0.002	0.038	Balance	

Experimental Setup

The material studied was a longitudinal weld bead obtained from X52 pipeline steel. Three different zones were studied, HAZ, WB and BM. This weldment was produced by the submerged arc welding process. All electrochemical tests were carried out in a 1L air-tight electrochemical glass cell with a three electrodes array. Working electrode (WE) was made according to different zones of the longitudinal weld bead. The WE used had the following total exposed areas: 1 cm^2 for WB specimens, 0.1 cm^2 for HAZ specimens and 1 cm^2 to BM specimens. Before each test, the WE was polished with silicon carbide (SiC) paper up to 600 grit, and then it was cleaned with deionised water, degreased with acetone and kept in a desiccator. The reference electrode used was a saturated calomel electrode (SCE) and a sintered graphite rod was used as auxiliary electrode (AE).

Electrochemical Measurements

The electrochemical measurements referred to SCE were:

a) Corrosion potential (E_{corr}) against time.

b) Linear Polarization Resistance (LPR). The potential range used was ±0.015 V referred to E_{corr} and a sweep rate of 0.001 Vs^{-1}. In all calculations of the corrosion rate, the experimental value of the Stern-Geary constant was considered.

c) Polarization curves (PCs) were recorded at a sweep rate of 0.001 Vs^{-1}, the potential range used was ±0.5 V referred to E_{corr}.

Electrochemical measurements were carried out at several time intervals during the exposure time. After exposure, selected samples were used in order to analyse the chemical composition of the corrosion products by Energy Dispersive X-Ray (EDX) emission analysis through a Scanning Electron Microscope (SEM) and X-Ray Diffraction (XRD).

Results and Discussion

Corrosion Potential, E_{corr}.

Fig. 1 shows the variation of the measured E_{corr} with the time exposition in the test solution without and with H_2S. In both conditions (NACE brine with and without H_2S), it is possible to observe that, the measured values of the E_{corr} corresponding to HAZ are more electronegative than E_{corr} values of the WB and BM.

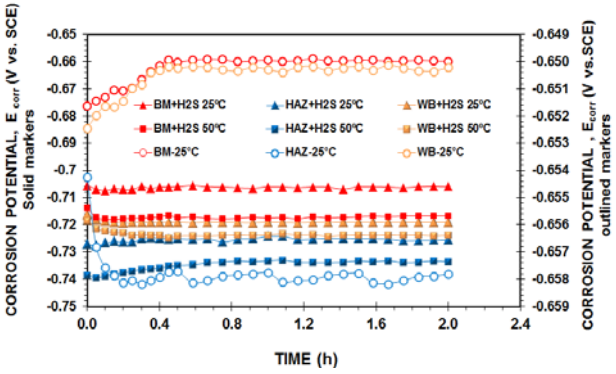

FIG. 1 E_{CORR} AS A FUNCTION OF TIME OF THE X52 STEEL IN TEST SOLUTION WITHOUT AND WITH H_2S AT 25°C AND 50°C

The E_{corr} values of the WB also are more electronegative than E_{corr} values of the BM. In addition, it is important to note that at 25°C, all values of the E_{corr} corresponding to NACE brine with H_2S are more electronegative than the E_{corr} values of the NACE brine without H_2S. This behaviour shows that the E_{corr} of the three weld zones of the carbon steel have been affected by the H_2S dissolved in the test environment.

Corrosion Rate, CR (LPR test)

Fig. 2 shows the variation with the time of the experimental CR values obtained in the LPR tests. It is clear that temperature affects the measured CR. In NACE brine with H_2S, CR rises as the temperature increases.

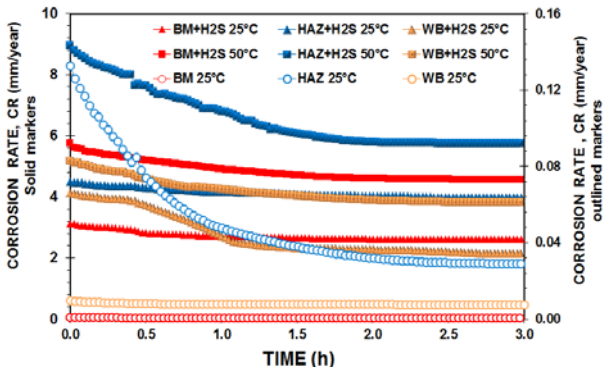

FIG. 2 CR CALCULATED BY LPR AS A FUNCTION OF TIME. X52 STEEL WELD IN TEST SOLUTION WITHOUT AND WITH H_2S AT 25°C AND 50°C.

This temperature effects is important because the transfer of electrochemical species from the bulk to surface of the X52 pipeline steel weld, FeS formation, and the charge transfer in the corrosion process (Arzola-Peralta, 2006) is promoted. At 25°C, the

highest CR was measured in the NACE brine with H_2S; and this behaviour could be attributed to the fact that H_2S gas can be dissolved in aqueous environment in which it can be turned into corrosive solutions (Galván-Martínez, 2004,2005; Seki, 1982).

It is important to point out that, in both brines (with and without H_2S), the highest CR was measured in the HAZ of the weldment and the CR of the WB zone is higher than BM zone. This behaviour could be attributed to the variation in the microstructure (grain size) and residual stresses (Sephton, 2000).

In addition, at the beginning of the test, all measured CR moves to higher values and as the exposure time increases, the CR changes to stable values. This behaviour can be due to the fact that at the beginning of the test, the surface of the steel was clean and consequently active. After a period of time, a corrosion product film was formed on the working electrode surface insulating partially the metal surface from the test solution, and reduced with this fact the corrosion rate. According to some researchers, the first product of the film formed in the corrosion of the steel in sour environment is meanly mackinawite (R. Galvan – Martinez, 2005; Videm, 1995; Vedage, 1993).

Polarization Curves (PCs)

Fig. 3 shows the PCs of the steel in NACE brine without and with H_2S at 25°C and 50°C. Table 3 presents the corrosion parameters calculated from the PCs. Fig. 3 shows that all corrosion current densities (i_{corr}) in NACE brine with H_2S at 50°C are higher than i_{corr} in NACE brine with and without H_2S at 25°C; consequently the calculated CR values have the same behaviour. It is important to point out that the cathodic branches in the PCs shown in figure 3a have slopes (0.18 V/decade aproximately) that can not be associated to a pure charge transfer (Galvan –Martinez, 2005). This feature suggests a contribution of a mass transfer process (mainly H^+) to the cathodic kinetics.

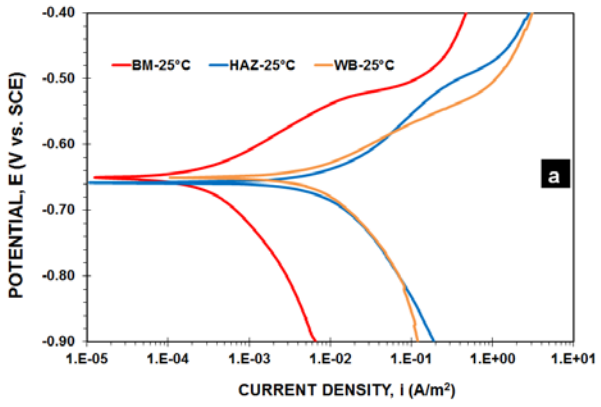

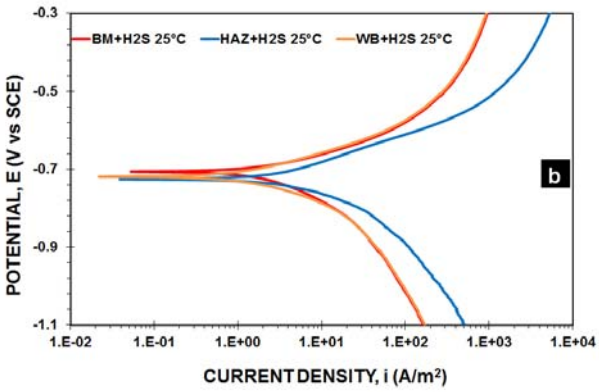

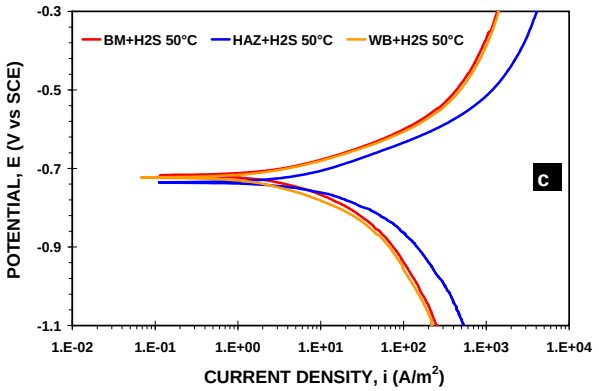

FIG. 3 PCs OF THE X52 STEEL WELD IN TEST SOLUTION WITHOUT (a) AND WITH H_2S AT 25°C (b) AND 50°C (C).

On the other hand, the PCs shown in figure 3b and 3c have cathodic branches that could be related with a charge transfer process. The corrosion parameter obtained by the polarization curves, and the corrosion rate calculated from these parameters can be observed in table 3. According to table 3, the CR values obtained by polarization curves has the same behaviour that the CR values obtained by LPR test; the CR increases as the temperature also rises and at 25°C, the CR values in NACE brine with H_2S are higher than those in NACE without H_2S. Finally, it is important to point out that the calculated CR values in HAZ are higher than those obtained in the BM and WB.

TABLE 3 CORROSION PARAMETERS OBTAINED FROM THE PCs SHOWN IN FIG. 3

Test Solution	Weld Zone	$B_{Exp.}$ (V)	i_{corr} (A / m²)	CR (mm/year)
NACE without H_2S at 25°C	BM	0.022	3.20E-04	0.00037
	HAZ	0.026	1.00E-02	0.01159
	WB	0.021	6.35E-03	0.00736
NACE with H_2S at 25°C.	BM	0.020	2.30E+00	2.66678
	HAZ	0.019	3.40E+00	3.94219
	WB	0.018	1.65E+00	1.91312
NACE with H_2S at 50°C.	BM	0.022	4.20E+00	4.86977
	HAZ	0.017	5.20E+00	6.02923
	WB	0.019	3.00E+00	3.47840

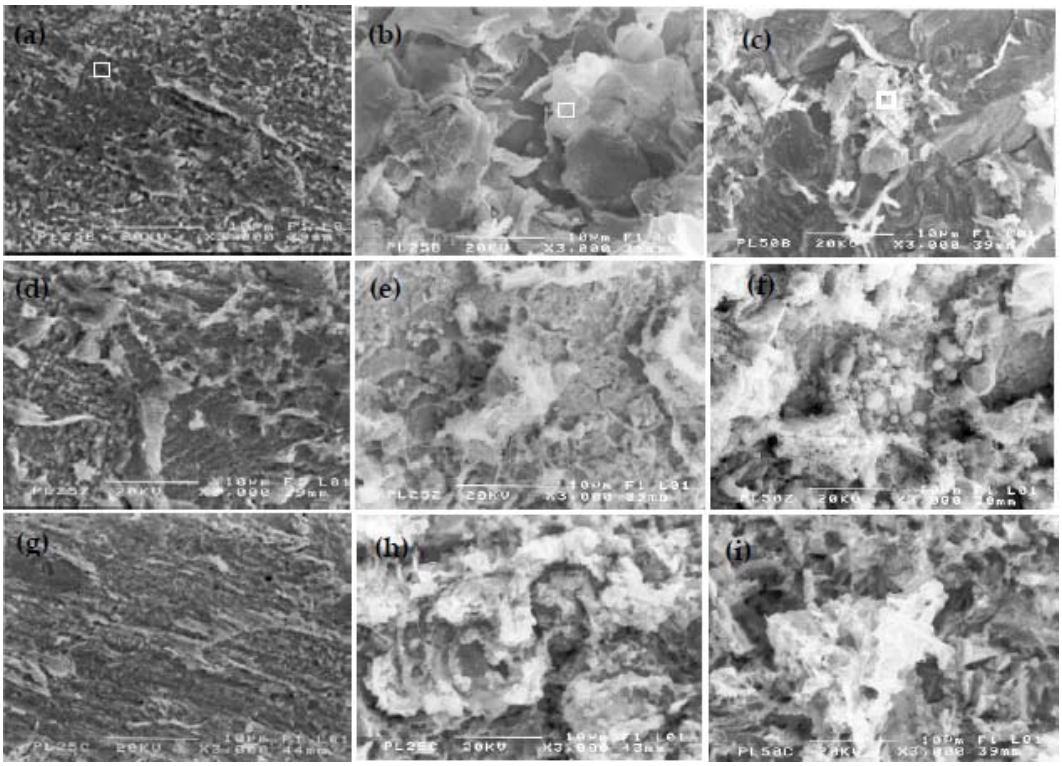

FIG. 4 SEM MICROGRAPHS OF THE CORROSION PRODUCTS FILM OBTAINED FROM THE WELDMENT EXPOSED TO THE NACE BRINE WITHOUT H_2S (a, d, g) AND NACE BRINE WITH H_2S AT 25°C (b, e, h) AND 50°C(c, f, i).

Surface Analysis

Fig. 4 shows a micrograph obtained by SEM from the three different zones of the weldment (Fig. 4a to 4c BM, Fig. 4d to 4f HAZ and Fig. 4g to 4i WB) exposed to the NACE brine solution without and with H_2S. These micrographs show the corrosion product film formed on steel surface at 25°C and 50°C and both condition (with and without H_2S). The squares shown in each micrograph indicate the analyzed area by SEM.

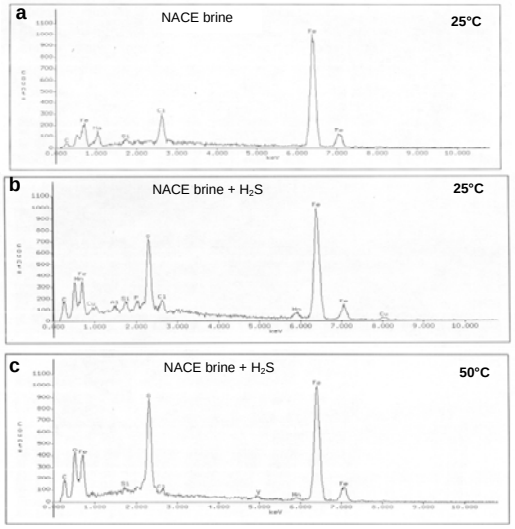

FIG. 5. CHEMICAL MICROANALYSIS OF THE BM EXPOSED TO NACE BRINE SOLUTION WITHOUT (5A) AND WITH H_2S AT 25°C (5B) AND 50°C (5C).

Fig. 5 shows a chemical microanalysis corresponding to the sample tested in NACE brine without H_2S (5a) and with H_2S at 25°C (5b) and 50°C (5c).

The chemical microanalysis was obtained from the sample of the BM. In Fig. 5a, the EDX spectrum shows that the two elements with major concentration in the corrosion products film are chloride (Cl) and iron (Fe). These elements constitute the iron chloride film formed in seawater environment (Mercer, 1990). According to XRD results obtained in samples tested at 25°C, lawrencite ($FeCl_2$) and molysite ($FeCl_3$) were the main corrosion products found.

In figures 5b and 5c, the EDX spectra show that the two elements with major concentration in the corrosion products film are sulphur (S) and iron (Fe). These elements constitute the iron sulphur film formed in H_2S environments. According to XRD results, mackinawite ($Fe_{1+X}S$) was the corrosion product found at 25°C. It is important to point out that, when the temperature increases at 50°C, mackinawite, Troilite (FeS) and Pyrrhotite ($Fe_{1-X}S$) were found. These results are agreed with the results obtained by some researchers (Shoesmith, 1980; Tewary, 1979; Wikjord, 1980; Pound, 1989) about the steel corrosion in aqueous solution containing dissolved H_2S.

Conclusions

The electrochemical measurements at 25°C show that

the CR calculated from the welding of the X52 steel in NACE brine with H_2S is higher than that calculated in NACE brine without H_2S. This fact can be attributed to the H_2S because it turns the NACE brine solution more corrosive. In general, in NACE brine with and without H_2S, the CR in HAZ is higher than that in the WB and as well the corrosion rate in WB is higher than that in the BM. This behaviour could be attributed to the variation in microstructure (grain size) and residual stresses. The CR in NACE brine with H_2S increases as the temperature also increases from 25°C to 50°C. This temperature effects promote the transfer of electrochemical species from the bulk to the surface of the welding of X52 pipeline steel and the charge transfer in the corrosion process. In NACE brine with and without H_2S at 25°C and 50°C, the calculated CR decreases with the increment of exposure time. This behaviour can be attributed to the formation of a corrosion products film on surface of the X52 pipeline steel weld. According to surface analysis, the corrosion product film that covered the surface of the X52 pipeline steel weld in NACE brine without H_2S at 25°C was iron chloride, whereas the sample in NACE brine with H_2S at 25°C and 50°C was iron sulphide. In addition, the iron sulphide formed on surface of the X52 pipeline steel weld at 25°C was mackinawite, and when the temperature increases from 25°C to 50°C, mackinawite, troilite and pyrrhotite were found.

REFERENCES

Arzola-Peralta, S., Mendoza-Flores, F., Duran-Romero, R., Genesca, J., Corros. Eng. Sci. Technol., 41, pp 321-327, 2006.

Borgne, S., Romero, J.M., Villalobos, Videla, H.A., MP, 46, p52, 2007.

Cayard, M. S., Kane, R. D., Corrosion, 53, pp227-233, 1997.

Cheng, X. L., Ma, H. Y., Zhang, , J. P., et- al, Corrosion, 54, pp 369-376, 1998.

Ewing, S. P., Corrosion, 11, pp 51-56, 1955.

Galván-Martínez, R., et al, Materials and Corrosion, 55, pp 586-593, 2004.

Galván-Martínez, R., et al, AFINIDAD, 62, pp 448-454, 2005.

Galvan-Martinez, R., et-al, Materials and Corrosion, 56, pp 678-684, 2005.

Huang, H. H., Tsai, W. T., Lee, J. T., Corrosion, 52, pp 708-713, 1996.

Li, J., et-al., CORROSION, 62, pp 316-322, 2006.

Loto, C.A., Matanmi, M.A., Brit. Corros. J., 24, p. 36, 1989.

Lu, B.T., Luo, J.L., CORROSION, 62, pp129-140, 2006.

Mercer, A.D., Corrosion in Seawater Systems, Ed. ELLIS HORWOOD, 1990.

Olsen, S., Sundfaer, B., Enerhaug, J., Proc. Conf. on Corrosion´ 97, National Association of Corrosion Engineers, Paper No. 43, 1997.

Perdomo, J.J., Morales, J.L., Viloria, A., Lusinchi, A.J., MP, 41, pp54-58, 2002.

Pound, B. G., Wright, G. A., Sharp, R. M., Corrosion, 45, pp 386-392, 1989.

Romero, J.M., Villalobos, J.L., Sosa,E., Amaya, M., CORROSION, 60, p689, 2004.

Seki, T. Kotera, T. Nakasawa, Proc. Conf. on Corrosion 82, National Association of Corrosion Engineers, Paper No. 131, Houston, TX, USA, 1982.

Sephton, M., Pistorius, P.C., Corrosion, 56, pp1272-1279, 2000.

Shoesmith, D. W., Taylor, P., Bailey, M. G., Owen, D. G., J. Electrochem. Soc., 127, pp 1007-10155, 1980.

Tewary, P. H., Bailey, M. G., Campbell, A. B., Corros. Sci., 19, pp 573-585, 1979.

Vásquez, R., Hazan, L., Uruchurtu, J., Malo, J.M., Genescá, J., 60, pp 136-143, 2003.

Vedage, H., Ramanarayanan, T. A., Mumford, J. D., Smith, S. N., Corrosion, 49, pp 114-121, 1993.

Videm, K., . Kvarekvål, J., Materials and Corrosion, 51, pp 260-269, 1995.

Wikjord, A. G., et al, Corros. Sci., 20, pp 651-671, 1980.

Wranglen, G. "An Introduction to Corrosion and Protection of Metals", Ed. Chapman and Hall Ltd., Printed in Great Britain, 1985

Dr. Ricardo Galvan-Martinez is a researcher of Anticorrosion group in the Engineering Institute of the Veracruzana University of Mexico since 2005. He has 15 years of experience as corrosion specialist mainly in the oil industry. He has a Bachelor´s degree in Biochemical Engineering, Master degree in Metallurgy and Materials Science and Ph.D. in Engineering with corrosion specialty. He is a member of NACE and NACE-certified of Internal Corrosion Technologist. Arbitrator of some International corrosion journal. He is author of many high-impact index papers about corrosion area and he belongs to National Research System, Level 1. Research areas: pipeline internal corrosion.

Dr. Melchor Salazar-Martínez. Researcher of the Mexican Institute of the Petroleum (from 2002) in the Program of Pipelines Integrity (until 2006) and the Program of Exploitation of fields in Deep Waters from 2006 in the materials area (pipe and risers for deepwater).

B.S. in Mechanical engineering, specialty and master degree in metallurgy and materials science. PhD in chemical sciences with specialty in metallurgy and material science, and he belongs to National System of Researchers, Level 1. Research areas: Materials for deepwater applications, SCC, SSC, HIC, prevention and analysis of failures.

Dr. Ricardo Orozco-Cruz is a researcher at the Anticorrosion Group in the Institute of Engineering, Veracruzana University, He has a Bachelor´s degree in Mechanical Engineering, M. S. degree in Materials Science and a Ph. D. in Engineering.

He has nine years of experience researching and teaching in the corrosion field. He is a member of NACE and Mexican Electrochemical Society. He is a NACE-certified CP Tester. He works in the areas of materials science and corrosion engineering. His research interest include marine corrosion, cathodic protection and now, the effects of climatic change on the marine infrastructure.

Dr. Miguel Angel Morales-Cabrera is a researcher of the University of Veracruz of Mexico since 2008. He has a Ph.D. in Chemical Engineering and a M.S. in Chemical Engineering by the Metropolitan Autonomous University of Mexico, his Bachelor's degree is in Chemical Engineering.

He is a member of the Mexican Academy of the Research and Teaching in Chemical Engineering. His main research interest includes analysis of the chemical engineering processes mainly in transport phenomena. However, his research interest also includes underground corrosion.

Dr. Antonio Contreras-Cuevas is a pipeline materials research specialist for Mexican Petroleum Institute since 2003. He has obtained a master degree in 1997 and PhD in 2002 in Metallurgy and Materials Science from National Autonomous University of Mexico (UNAM).

He is a member of NACE and Mexican Materials Society, and he belongs to National Research System (SNI-level 2). The main research areas include stress corrosion cracking (SCC), root cause analysis (RCA), materials characterization and pipeline integrity.

doi: 10.14355/jpsr.2013.0204.03

Pressure Transient Analysis of Multi-stage Hydraulically Fractured Horizontal Wells

Fei Wang*[1], Shicheng Zhang[2], Bailong Liu[3]

*[1]Institute of Petroleum Engineering, China University of Petroleum, Beijing, 102249, China
[2]Institute of Petroleum Engineering, China University of Petroleum, Beijing, 102249, China
[3]Institute of Petroleum Engineering, China University of Petroleum, Beijing, 102249, China

*[1]wangfei@cup.edu.cn

Abstract

The horizontal well with multiple transverse fractures has proven to be an effective way to exploit tight reservoirs economically. Due to the nature of ultralow permeability, it would take a significant long period of time for a well producing in transient flow regimes. Therefore, pressure transient analysis for such a well is important in both evaluation of fracturing treatment by estimating fracture and reservoir parameters and prediction of the long-term production behavior of wells in oil recovery. This paper discusses the analysis of pressure-transient responses of horizontal wells intercepting multiple infinite-conductivity transverse fractures. Then a numerical model is utilized to simulate the whole well flow regimes and pressure transient characteristics of multiple fractured horizontal wells. Accordingly, appropriate analytical pressure-transient models and analysis procedures are provided to determine fracture properties, i.e. average fracture half-length and spacing and estimate the oil in place in the stimulated reservoir volume.

Keywords

Pressure Transient; Multiple Fractured Horizontal Wells; Analytical Models; Stimulated Reservoir Volume

Introduction

Currently, economic extraction of hydrocarbon from tight formations is featured by completion of a long horizontal lateral intersected with multiple transverse fractures (Yost, A.B. and Overbey, W.K., 1989). Pressure transient characteristics and analysis of fractured horizontal wells have been discussed in several studies. Larsen and Hegre (1991 and 1994) studied pressure transient behavior of a horizontal well with transverse fractures and provided description of pressure-transient flow regimes with corresponding analytical solutions. Al-Kobashi et al (2006) concentrated on the pressure-transient characteristics at the early-time flow regimes. They described the fracture storage induced flow regimes for the multiple transverse fractured horizontal wells (MTFHW) including fracture-radial, radial-linear flow and bilinear linear flow. In their literatures, the early time corresponding to the period prior to the start of the interference between fractures was considered. Since the fracture interference is negligible, the pressure response of the MTFHW was correlated with the single fracture responses. Zerzar et al (2004), Clarkson et al (2009) and Freeman et al (2009) concentrated on the pressure-transient characteristics at relatively later times (after the end of fracture-storage), and described flow regimes for the MTFHW including pseudo-linear flow, pseudo-radial and compound linear flow(or bi-radial flow) before infinite-acting, pseudosteady state or steady state flow related to the extent of the well drainage area. Song et al (2011) introduced the term pseudo pseudosteady state for the flow regime between pseudolinear flow and compound linear flow.

Because the matrix permeability of tight formations is extremely low, like shale typically in a range of tens to hundreds of nano-darcy, the permeability of hydraulic fractures with milli-darcy scale dominates the transient flow. And then the fracture interference dominated flow regimes take more time in consequence. In this paper, we concentrated on the pressure transient response at the fracture interference dominated flow regimes. In order to ensure the coherence, we studied the entire pressure transient behavior of the MTFHW in tight formations and provided description of pressure-transient flow regimes with corresponding analytical solutions. Numerical synthetic cases have proved our analytical models and analysis procedures.

Pressure Transient Mathematical Model

We consider the flow of a slightly compressible liquid in a bounded reservoir that is in the form of a rectangle. The porous medium is assumed to be homogeneous system and may exhibit simple

anisotropy. Each fracture that intercepts the horizontal wells has same properties, i.e. length, width, permeability and porosity are identical. All fractures produce against a wellbore pressure that may be a function of time under the constant-rate. Such a model can be used to analyze the production or test data from multiple fractured horizontal wells.

For the mathematical model considered here, in the absence of wellbore storage effects, four major flow periods to control the well pressure response are expected provided that the fracture-storage induced flow period is non-exist: (1) an early-time flow period wherein the system behaves as if it were an n-layer, commingled reservoir where n is the total number of fractures, (2) an intermediate-time flow period that reflects interference effects between fractures, (3) a late-time flow period during which the composite fracture system behaves as if it were a single fracture equal to the spacing between the outermost fractures, and (4) finally reservoir boundary dominated flow period.

MTFHW Flow Regimes

To set the stage for our discussion on the analysis of pressure-transient responses, here a summary of the flow regimes of multiple fractured horizontal wells is presented (sketched in Fig. 1). Each of the regimes shown in Fig. 1 is discussed below.

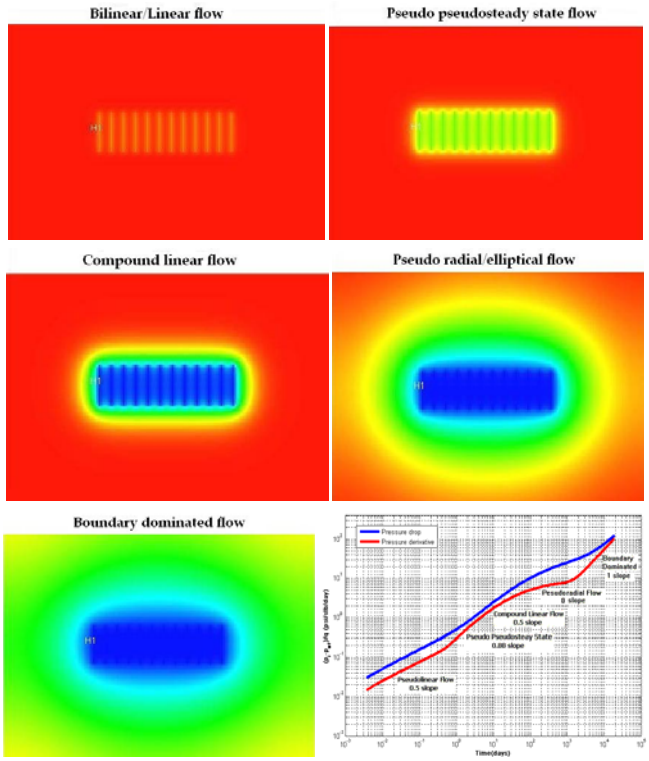

FIG. 1 SCHEMATIC OF MTFHW FLOW REGIMES (SIMULATION WITH ECLIPSE)

Early-time Linear or Bi-linear Flow

In this flow period, fluid flows down the fracture and flow in the reservoir is normal to the fracture planes. The type of flow regime (linear or bilinear) that dominates this period will depend on the fracture conductivity and length. Flow across the fracture tips is negligible and each fracture behaves independently of the other fracture.

Pseudo-Pseudosteady State Flow

During this flow regime, pressure interference between fractures dominates while the flow across the boundary between the inner and the outer stimulated reservoir volume(SRV) starts but insignificant. It is an approximate pseudo-steady state flow, with which the inner SRV is depleted with limited contribution from the outer SRV.

Compound Linear flow

During this regime, fracture interacts. The system behaves as if flow takes place to a fractured well that is parallel to the azimuth of the horizontal well. The flow pattern is predominantly normal to the vertical plane that contains the horizontal well.

Pseudoradial Flow

In this period, flow across the tips of the horizontal well becomes dominant and the flow pattern is similar to that of the long-term behaviour of vertically fractured wells.

Boundary Dominated Flow

This flow period occurs when the reservoir boundary is reached. In the case of closed boundaries, the flow will eventually reach pseudo-steady state.

The flow regimes presented above may not exist in a single test. Depending on the specific properties of the fracture and reservoir, some of the flow regimes may be absent. For the moderate ratios of fracture length and spacing, the pseudo-pseudosteady state flow regime may be nonexistent or replaced by a transitional period, such as bi-radial flow regime. It is possible that the pseudoradial flow regime may not exist because of well interference or boundary effects. Methods to analyze pressure data are presented below.

Straight-Line Analysis of Pressure-Transient Responses

For the mathematical model and flow regimes discussed above, straight-line analysis techniques can

be used for the estimation of the fracture properties and the oil in place in the stimulated reservoir volume. In this section, pressure transient equations dominating each flow regime will be presented. And then we will demonstrate the use of the straight-line analysis for the pressure responses of multiple fractured horizontal wells.

Early-time Linear Flow

The pressure response during the early-time linear flow period is given by

$$\Delta p_{wf} = 4.0641\frac{qB}{nhx_f}\sqrt{\frac{\mu t}{k\varphi c_t}} + \frac{141.2qB\mu}{kh}\left[s + s_p\right] \quad (1)$$

where s is the fracture surface skin and s_p is a pseudoskin factor that accounts for the additional pressure drop due to finite conductivity, flow choking, and fracture geometry. The early-time fracture linear flow period is characterized by a ½ slope straight line on a log-log plot of the derivative responses.

Based on Eq.1, a plot of pressure drop versus square root of time yields a straight line with a slope of

$$m_{fl} = 4.0641\frac{qB}{nhx_f}\sqrt{\frac{\mu}{k\varphi c_t}} \quad (2)$$

and as in the case of multiple fractured horizontal wells, the fracture half-length x_f can be obtained from Eq.2 if the formation height and reservoir permeability are known. The time at the end of early-time linear flow occurs when flow to adjacent fractures interferes. The time of this occurrence is given by

$$t_e = \frac{x_s^2\varphi\mu c_t}{4*(0.029)^2 k} \quad (3)$$

where x_s is the fracture spacing in ft.

Pseudo Pseudo-Steady State Flow

As indicated before, the pressure behaviour during the pseudo pseudo-steady state flow period is similar to the pseudo-steady state flow, with which the inner fracture is depleted with limited contribution from the outer fracture. The pressure drop during this flow regime is given by

$$\Delta p_{wf} = \frac{qBt}{24V_p c_t} + \Delta p_{\text{int}} \quad (4)$$

where Δp_{int} is the longitudinal intercept when plotting pressure drop versus time and yields a straight line with a slope of

$$m_{qf} = \frac{qB}{24V_p c_t} \quad (5)$$

Thus, the SRV pore volume V_p can be obtained from Eq. 5.

Pseudoradial Flow

The dimensionless pressure behavior during the intermediate-time pseudoradial flow period is similar to the line-source solution in a homogeneous reservoir with an additional pressure drop because of the effect of transverse fractures. The pressure drop during this flow regime is given by

$$\Delta p_{wf} = \frac{162.6qB\mu}{kh}\left[\log\left(\frac{2.64\times10^{-4}kt}{\varphi\mu c_t r_w'^2}\right) + \frac{s+s_p}{1.1516} + 0.3513\right] \quad (6)$$

Based on Eq. 6, the slope of the semi-log straight line during pseudoradial flow is given by

$$m_{pl} = \frac{162.6qB\mu}{kh} \quad (7)$$

Thus, the formation permeability *k* can be calculated directly from Eq. 7.

Pseudo-Steady State Flow

The pressure drop during the pseudo-steady state flow regime is given by

$$\Delta p_{wf} = \frac{qBt}{24V_r c_t} + \Delta p_{\text{int}}^{*} \quad (8)$$

where $\Delta p_{\text{int}}^{*}$ is the longitudinal intercept when plotting pressure drop versus time and yields a straight line with a slope of

$$m_{ql} = \frac{qB}{24V_r c_t} \quad (9)$$

Thus, the reservoir pore volume V_r can be obtained from Eq. 9.

Straight-Line Analysis Example

We now use a synthetic example to demonstrate the straight-line analysis of pressure transient responses of the MTFHW. The synthetic dataset used in the study is generated by a numerical model, considering a horizontal well intersected by multiple transverse fractures with identical properties. The modeled fractures are considered to be rectangular, vertical and transversal relative to well direction. Infinite conductivities are considered in this study. The wellbore hydraulics is honored by a multi-segmented wellbore model. The reservoir simulation cells are connected to the wellbore model using conventional techniques. Skin at each interface between reservoir cells and the wellbore model is assumed to be zero. The model considers the production of single-phase oil from an isotropic formation. The hydraulic fracture is modeled with Local Grid Refinement (LGR) technique. A series of thin blocks within LGR is assigned with the

properties of hydraulic fractures.

To test this particular grid model, a horizontal well model with 12 hydraulic fractures 60 ft equally spaced has been constructed. This allows the early time pressure transient behavior to be captured. Bottomhole pressure is simulated for 1000 days of production while a constant rate is specified in the model. A small rate is required to drain the tight formation with physically feasible bottomhole pressures. Basic reservoir and well data are listed in Table 1.

TABLE 1 PROPERTIES OF RESERVOIR, FLUID AND FRACTURE FOR THE EXAMPLE

Initial reservoir pressure	2550 psia
Total compressibility	3e-4 pis-1
Matrix porosity	0.0455
Matrix permeability	3e-3 md
Initial oil density	62.47 lb/ft3
Initial oil viscosity	1.25 cp
Formation thickness	30 ft
Fracture half-length	100 ft

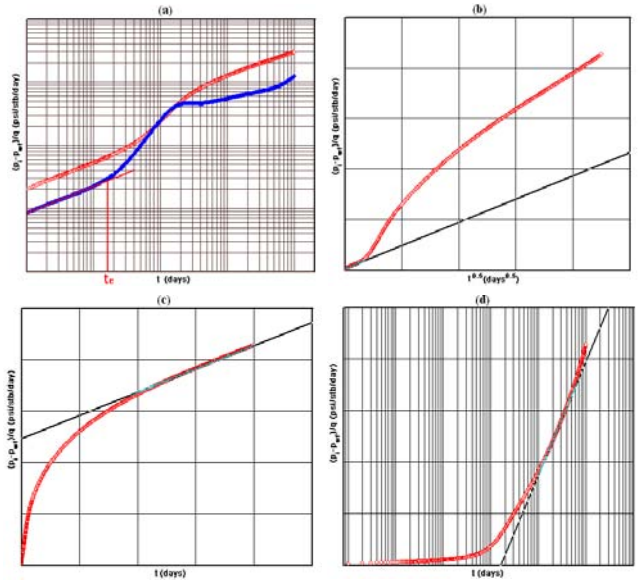

FIG. 2 STRAIGHT-LINE ANALYSIS PLOTS OF THE SIMULATED DATA IN THE EXAMPLE

Fig. 2(a) shows a log-log diagnostic plot of the data to be analyzed in this example. It can be seen from Fig. 2 that the early-time linear flow period (0.5-slope on derivative responses) is followed by the pesudo pesudo-steady state flow (0.88-slope on derivative responses) and an almost pseudoradial flow (0-slope on derivative responses). At late time, the pressure derivative goes upwards which reflects the reservoir boundary effect.

A plot of $\Delta p / q$ vs. the square-root-of-time during the early-time linear flow period, shown in Fig. 2(b), yields a straight line with slope m_{fl}. Using Eq. 2 with the data in Table 1, the fracture half-length x_f is calculated to be 107.16 ft. With the end point of linear flow, $t_e = 2$ days on log-log plot in Fig. 2(a), using Eq. 3 and the data in Table 1, the fracture spacing x_s can be calculated as 59.57 ft.

A Cartesian plot of $\Delta p / q$ vs. time during the pesudo pesudo-steady state of the fracture system shown in Fig. 2(c), yields a straight line with slope m_{qf}. Using Eq. 5 with the data in Table 1, the stimulated reservoir volume is calculated to be $6.3*10^6$ ft^3.

Note from Fig. 2(a) that the pseudoradial flow behavior is evident from the flat derivative responses before reaching the reservoir boundary. Thus, the plot of $\Delta p / q$ vs. the logarithm of time, shown in Fig. 2(d), yields a straight line with a slope of m_{pl}. Using this slope and Eq. 7 with the data given in Table 1, the formation permeability k, is calculated to be 0.0036 md.

Conclusions

In this paper, we have studied the pressure transient behavior of multiple infinite-conductivity transverse fractures intercepted by a horizontal well. Five basic flow regimes of a MTFHW have been identified and equations have been provided for specialized analysis of pressure and pressure derivative plot. A calculation procedure has been presented with a numerical synthetic case, which demonstrated that the early-time linear flow before the occurrence of fracture interference and the fracture interference dominated pseudo pseudo-steady state flow regimes are key to the analysis due to estimates for the fracture properties and the oil in place in the SRV heavily depending on these two flow regimes.

ACKNOWLEDGMENT

The author would like to thank Scientific Research Foundation of China University of Petroleum, Beijing (No.KYJJ2012-02-27) for the financial support during this research.

REFERENCES

Al-Kobaisi, M. "Pressure-Transient Response of a Finite-Conductivity Fracture Intercepted by a Horizontal Well." MSc Thesis, Colorado School of Mines, Golden, CO 2005.

Al-Kobaisi, M., Ozkan, E., Kasogi, H., and Ramirez, B. "Pressure-Transient Analysis of Horizontal Wells with

Transverse, Finite-conductivity Fractures." Paper PETSOC 2006-126 presented at the Petroleum Society's 7th Canadian International Petroleum Conference (57th Annual Technical Meeting), Calgary, Alberta, Canada, 13-15 June, 2006.

A. Zerzar, D.Tiab and Y.Bettam "Interpretation of Multiple Hydraulically Fractured Horizontal Wells." SPE 88707, presented at the 11th Abu Dhabi International Petroleum Exhibition and Conference, Abu Dhabi, U.A.E., 10-13 October, 2004.

Clarkson, C.R., Jordan, C.L., Ilk, D., and Blasingame, T.A. "Production Data Analysis of Fractured and Horizontal CMB Wells." Paper SPE 125929 presented at the 2009 SPE Eastern Regional Meeting, Charleston, West Virginia, 23-25 September, 2009.

Larsen, L. and Hegre, T.M. "Pressure-Transient Behavior of Horizontal Wells with Finite-Conductivity Fractures." SPE 22076, presented at the SPE International Arctic Conference, Anchorage, AK, May 29-31, 1991.

Larsen, L. and Hegre, T.M. "Pressure Transient Analysis of Multifractured Horizontal Wells." SPE 28389, presented at the SPE Annual Technical Conference and Exhibition, New Orleans, LA, Sept. 25-28, 1994.

Ozkan, E, Brown, M., Raghavan, R., and Kazemi, H. "Comparison of Fractured Horizontal-Well Performance in Conventional and Unconventional Reservoirs."Paper SPE 121290 presented at the SPE Western Regional Meeting, San Jose, California, 24-26 March, 2009.

Raghavan, R.S., Chen, C. and Agarwal, B."An Analysis of Horizontal Wells Intercepted by Multiple Fractures."SPE Journal 2 (3):235-245. SPE-27652-PA, 1997.

Song, B., Economides, M.J., and Ehlig-Economides, C.A. "Design of Multiple Transverse Fracture Horizontal Wells in Shale Gas Reservoirs." Paper SPE 140555 presented at the 2011 SPE Hydraulic Fracturing Technology Conference, Woodlands, TX, 24-26 January, 2009.

Yost, A.B. and Overbey, W.K. "Production and Stimulation Analysis of Multiple Hydraulic Fracturing of a 2,000 ft Horizontal Well." SPE 19090, presented at the SPE Gas Technology Symposium, Dallas, TX, June 1989.

Nomenclature

B = formation volume factor, rb/stb

r_w = well radius, ft

c_t = total compressibility, 1 /psia

h = formation thickness, ft

k = formation permeability, md

s = fracture skin factor, dimensionless

s_p = pseudoskin factor, dimensionless

x_s = fracture spacing, ft

x_f = fracture half-length, ft

Δp_{wf} = drawdown pressure drop, psia/day

q = flow rate, stb/day

t = time, hours

t_e = end of early-time linear flow, hours

n = fracture number, dimensionless

ϕ = porosity, fraction

μ = viscosity, cp

V_p = SRV pore volume, ft^3

V_r = Reservoir pore volume, ft^3

Journal of Petroleum Science Research (JPSR) Volume 2 Issue 4, October 2013 www.jpsr.org
doi: 10.14355/jpsr.2013.0204.04

A Review on SPE's Comparative Solution Projects (CSPs)

Akand W. Islam*1, Kamy Sepehrnoori2

Department of Petroleum and Geosystems Engineering
The University of Texas at Austin, TX 78712, USA

*1 awislam@utexas.edu; 2kamys@mail.utexas.edu

Abstract

The SPE's Comparative Solution Projects are very recognized suites of test datasets for specific problems and the hub of conducting independent comparison of reservoir simulation from different dimensions. The first one of this kind of projects was initiated in 1981 by Aziz S Odeh in order to compare solutions to a three-dimensional black-oil reservoir simulation problem obtained from different participants. Later, more nine independent CSPs were led by many investigators to examine other challenging problems of reservoir engineering. The aim of this article is to present an overview of these ten projects with brief description of the problems studied, the participants of each project, simulators or the solvers used, and any substantial differences of results obtained by the contributors found in any project.

Key words

Comparative Solution Project; SPE Reservoir Simulation; Case Studies; Black Oil; Compositional; Horizontal Well; Dual Porosity

List of Acronyms

AIM	Adaptive Implicit
BHP	Bottom Hole Pressure
CMG	Computer Modeling Group
EOS	Equation of State
FVF	Formation Volume Factor
GOR	Gas Oil Ratio
PVT	Pressure Volume Temperature
RSRC	Reservoir Simulation Research Corporation
SSI	Scientific Software Intercomp
SSC	Scientific Software Corp
SMC	Simulation and Modeling Consultancy, Ltd
TDC	Todd, Dieritch, and Chase, Inc
WAG	Water Alternating Gas
WOR	Water Oil Ratio

Introduction

The SPE Comparative Solution Projects (CSPs) is the attempt to provide independent comparison of methods and the renowned suite of test datasets for specific problems. This is designed to measure the state-of-the-art simulation capability for challenging and most up to date problems. Ten CSPs were completed in series. In each of projects, several commercial oil companies, software companies, research institutes, universities, and so on participated voluntarily. Aziz S. Odeh (1981) first started this project, which later incited considerable interest. Therefore, the SPE recommended to undertake the ongoing project. In this endeavor, in 1982 SPE Symposium on Reservoir Simulation, Khalid Aziz suggested to perform a comparison of results on another test problem. Upon his proposal, H. G. Weinstein and his co-workers organized second CSP (Weinstein and Chappelear, 1986). The enthusiastic response of industry and the academic community encouraged this kind of project to be continued from one after another. The problems in these projects are designed by one or more knowledgeable people, and model results are provided directly by those who have built or acquired suitable models. This is different from a study where the person doing the comparison develops new software using published descriptions of several models and simulators. The projects were focused on the simulators of black-oil, coning, gas cycling, steam injection, miscible flood, dual porosity, and horizontal wells. The study for the black oil simulation was reexamined. The techniques on gridding and upscalling were compared among different simulators.

In this paper, an overview of all the completed CSPs has been made. For each of the individual projects, brief description of the problem statements, number of participants, types of solvers/simulators used was presented. However, details of results were avoided for brevity. Any major discrepancies found in comparisons of any project were highlighted. Possible reasons behind the disagreements of the results were attempted to be addressed.

Ten CSP's: at a Glance

Table 1 shows the research areas on which previous ten CSPs were carried out. Number of participants is also reported in this table. Descriptions of each of these projects are illustrated in following subsections.

First SPE-CSP

The first project (Aziz Odeh, 1981) involved a three layer black-oil simulation with gas injection into the top layer. Along with stratification and reservoir properties, areal and cross section views were given. The reservoir initially was assumed to be undersaturated. All pertinent data and constraints, PVT properties, relative permeabilities, etc. for the simulation inputs were supplied. Upon solving the problem, the participants were asked to report oil rate vs. time, GOR vs. time, the pressures of the cell where the injector and producer are located, gas saturation, cell pressures, and saturation pressures for the variable saturation-pressure case. Both constants and variable bubble point pressure assumptions were accounted for solving the problems. Seven companies participated in this project. Computers and the models used are shown in Table 2. Other than some little variations, all model predictions from all parties were in fair agreement. The small variations were due to the use of different numerical schemes, number of grid cells, and upstream techniques etc. No simulator performance data like run times, timestep size, profiling history were reported.

TABLE 1 CONCENTRATION OF TEN CSP's

Project no.		Concentration	No. of participants
1.	CSP-1	Three-Dimensional Black-Oil Reservoir Simulation Problem	7
2.	CSP-2	A Three-Phase Coning Study	11
3.	CSP-3	Gas Cycling of Retrograde Condensate Reservoirs	9
4.	CSP-4	Steam Injection Simulation	6
5.	CSP-5	Miscible Flood Simulation	7
6.	CSP-6	Dual-Porosity Simulation	10
7.	CSP-7	Modeling of Horizontal Wells in Reservoir Simulation	14
8.	CSP-8	Gridding Techniques in Reservoir Simulation	5
9.	CSP-9	Black-Oil Simulation (reexamination of CSP-1)	9
10.	CSP-10	Upscaling Techniques	9

TABLE 2 FEATURES OF SPE-CSP 1

Participants	Computer used	Method used	Name of Simulator	Comment
1. Amoco Production Co.	IBM 3033, IBM 370/168, and Amdahl V/6	IMPES		Their method is proved to be quite satisfactory; additional computations for implicit handling of interblock flow were not needed.
2. Computer modeling group of Calgery (CMG).	Honeywell 600 DPS	Fully implicit		The model is fully implicit in its basic formulation. When the options for two point upstream or centralized upstream weightings are used or when multiblock completion wells are modeled, the method becomes highly implicit but not fully.
3. Exxon Production Research Co.	Amdahl 470/V5 and IBM 370/168	Sequential Implicit Solution (Spillete et al., 1973)	GPSIM	GPSIM can account for reservoir heterogeneity, rock compressibility, and solution of gas in both oil and water. It can model vaporization of oil into the gas phase and hysteresis in the capillary pressure and relative permeability. The minor restriction is that it has the number of grid blocks can be used; large problems can be run using only relatively modest amounts of central memory.
4. Intercomp Resource Development and Engineering Inc.	Cray-1 and Harris/7		BETA II Black-Oil	BETA II has a large variety of user oriented features. It can solve for both saturations explicitly (IMPES) and either or both saturations implicitly (sequential).
5. Mobil Research and development Corp.	CDC Cyber 175		ALPURS (Bansal et al., 1979)	ALPURS is a three- dimensional, three phase, multiwell, black-oil reservoir simulator which uses a strongly coupled, fully implicit method to solve simultaneously all unknowns.
6. Shell Development Co.	Univac 1110/2C Level 36	IMPES or implicit mode		There are several indirect and direct solution methods as a user option. Additionally, two-point upstream weighting is used to calculate phase mobilities.
7. Scientific Software Corp (SSC).	CDC Cyber 175	AIM (Adaptive Implicit Method)		This technique developed at SSC, seeks to achieve an optimum with respect to stability, truncation errors, and computer costs. This simulator also provides a wide variety of user oriented features (Thomas and Thurnau, 1982)

TABLE 3 FEATURES OF SPE-CSP 2

Participants	Method used	Name of Simulator	Comment
1. Arco Oil and Gas Co.	Arco's two coning simulators are implicit, three-phase, Black-oil simulators.		The numerical formulation in both versions is a linearized semi-implicit scheme with upstream weighting for phase mobilities. Within a timestep, only the nonlinear accumulation term is updated if necessary. The algebraic equations are solved directly. The D4 reordering scheme was used to improve efficiency (Price and Coats, 1974). Three-phase relative permeabilitis are calculated by Stone's method (Stone, 1970, 1973).
2. Chevron Oil Field Research Co.	General-purpose Black-oil reservoir simulator.	CRS-3D	The program performs a fully implicit, simultaneous calculation of pressure, saturation, and wellbore BHP. This method used finite-difference discretization.
3. D&S Research Development Ltd.		The D&S Simulator	This is a fully implicit, 3D, three phase program that solves simultaneously for all unknowns. The systems of equations are solved by ITD4MIN techniques (Tan and Lakeman, 1982).
4. Franlab Consultant, S. A		The Franlab Simulator (Sonier et al., 1973)	This is a 2D, three-phase program based on finite difference techniques.
5. Gulf Research and Development Co.	Black-Oil		The Gulf black-oil coning model employs standard point centered spatial differencing and fully implicit backward time differencing.
6. Harwell	General-purpose implicit, three-phase, 3D Black-oil Simulator	PORES (Cheshire et al., 1980)	This contains an extensive well model that is numerically stable, meets production targets precisely, and approaches flows accurately to individual layers of the reservoir model.
7. Intercomp.	Implicit flow model		This model simulates one-, two-, or three-dimensional isothermal flow of three phases in Cartesian or cylindrical coordinates.
8. McCord-Lewis Energy Services.	General Purpose 2D model.		This model employs an FVF PVT description with a variable saturation pressure feature. Relative permeability approximations are semi-implicit (extrapolated over the time step), and finite-difference equations are solved sequentially.
9. J. S. Nolen and Assocs.	VIP (vectorised implicit program), a general purpose, 3D, three-phase black-oil simulator (Nolen and Stanata, 1981; Stanata and Nolen, 1982).		VIP efficiently solves both single-well and field-scale production problems. This is fully implicit in saturations and bubblepoints and uses a modified Newton-Raphson iteration to solve simultaneously for three unknowns per gridblock.
10. SSC.	same as in Table 2.		
11. Shell Development Co.		The Shell isothermal reservoir simulation system (Chapplear and Rogers, 1974).	This operates either in an IMPES or semi-implicit mode.

TABLE 4 FEATURES OF SPE-CSP 3

Participants	Computer used	Method used
1. Arco Oil and Gas Co.	IBM 4341	IMPES
2. Chevron oil Field Research Co.	VAX-11/780	same
3. Core Laboratories Inc	CDC 6600	same
4. CMG	Honeywell DPS 68	same
5. Soc. Natl. Elf Aquitaine.	IBM 3081	same
6. Intercomp (now Scientific Software-Intercomp)	Harris 800	same
7. Marathon Oil Co.	Burroughs B7900	same
8. Mccord-Lewis Energy Services.	VAX-11/780	same
9. Petek, The Petroleum Technology Research Inst.	ND-560	same

Second SPE-CSP

After successfully completing the first project, Aziz Odeh suggested that extension of the cooperative effort started with the publication on first CSP to cover more complex models and problems would be very beneficial to the industry, as well as that the SPE continues such an attempt. Khalid Aziz then recommended organizing a comparison of results on another test problem during the organization of the 1982 SPE Symposium on Reservoir Simulation. Since first CSP had been a field-scale simulation, a coning

study was thought to be of interest. To this end, a problem drawn from an actual field case was simplified somewhat to provide a challenging test problem (Weinstein et al., 1986). It was a single-well radial cross section that involved gas and water coning as well as gas repressuring, meanwhile a difficult problem which provided a good test of the stability and convergence behavior of the simulators. Name of participants and the simulators used are as follows in Table 3. Surprisingly the numerical results obtained agreed well though there was diversity of discretization and solution methods used. Some participants remarked that the problem was rather impractical because rate variations mentioned in problem statements would not be likely to occur. More so, the solution GOR was unusually high for oil with a high density. These cases made the problem more difficult to solve, representing a mere test of simulation techniques.

Third SPE-CSP

The problem in third CSP (Kenyon and Behie, 1987) selected was to study gas cycling in a rich-gas retrograde condensate reservoir. Numerical comparisons of the PVT data match were considered important. Computational speed of the simulators was not to be of concern. In the first part of the study, the participants matched their phase-behavior packages to the data supplied, and in the second part they considered two options for the depletion of the reservoir. This study required a 3D, three-phase, multicomponent compositional model. Nine companies participated in this study introduced in Table 4. The participants were asked for matches of total volume in constant–composition expansion, liquid dropout and equilibrium gas yield in constant-volume depletion, and swelling volume and dewpoint pressure during swelling of reservoir gas with lean gas. In addition, they were requested to describe techniques used for equilibrium *K* values, phase densities and viscosities, and EOS parameters used for the PVT match. A 16 component PVT simulator was used to prepare *K* value data by convergence pressure techniques. Slight heavy – component *K*-value adjustment was used to match dewpoint pressures, liquid volumes, and depletion-gas compositions. The two major parts of a compositional model study were the PVT data and the reservoir grid, respectively. For the PVT data, participants were supplied with a companion set of fluid analysis reports. The specification of the reservoir model and the grid were given. In comparisons of results: depletion data and lean-gas swelling data for the retrograde gas condensate matched well by all participants. In early years of cycling with partial pressure maintenance, the surface oil rates disagreed by about 20%. Probably, differences in pressure caused by physical property errors (*Z* compressibility factors) and/or surface–separator molar split errors were responsible for the discrepancies. Large discrepancies (as shown in Figure 1) were observed in incremental oil obtained by gas-sales deferral; and the range was 3 to 8% of initial condensate in place. There was considerable disagreement about condensate saturation in the producing node. This was probably because *K* values were used as tables or as calculated in line with an EOS.

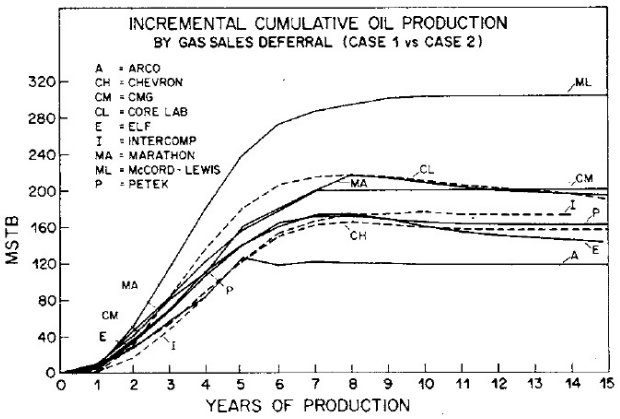

FIG. 1 INCREMENTAL RESERVOIR MODEL STOCK-TANK OIL PRODUCED BY GAS-SALES DEFERRAL (Kenyon and Behie, 1987)

Fourth SPE-CSP

The fourth CSP conducted by Aziz et al., (1985) was a two-dimensional radial steam injection (thermal) simulation, in which there are three related but independent problems for the comparison of steam injection models: (1) cyclic steam injection in a nondistillable oil reservoir with a 2D radial cross-sectional grid, (2) nondistillable oil displacement by steam in an inverted nine-spot pattern by considering one-eighth of the full pattern, and (3) displacement of an oil consisting of two volatile components and one nonvolatile component in the same patterns as problem 2. The oil properties were the same in first two problems. The participants had the flexibility to submit results for one, two, or all three problems. These problems were selected to exercise features of the models that are considered to have practical applications though they do not represent real field simulations. Six companies (shown in Table 5) participated in this project with only three submitting results for the compositional case (problem 3). The authors (Aziz et al., 1985) discussed the models used

comprehensively with some minor editorial change of originally submitted reports by the companies. The results submitted were mostly in good agreement except some significant differences. Possible reasons can be included as handling of interblock terms in the model, handling of wells, different convergence tolerance set, timestep selection, heat-loss computation process, different program control parameters, errors in data entry, nine point data entry used, possible bugs in the program, etc.

TABLE 5 FEATURES OF SPE-CSP 4

	Participants	Method used	Comment
1.	Arco Oil and Gas Co.	Scinetific Software-Intercomp's (SSI's) THERM model.	SSI's THERM is 3D generalized numerical simulation model applicable to design and analysis of projects involving steam flooding and cyclic stimulation and in-situ combustion. The model's optional nine-point difference scheme (Yanosik and McCraken, 1979; Coats and Modine, 1983) reduces grid-orientation effects associated with the conventional five-point scheme (Todd et al., 1972; Coats and Ramesh, 1986).
2.	Mobil R&D Corp.	same	same
3.	SSI.	same	same
4.	Chevron Oil Field Research Co.	IMPES	Chevron's steamflood simulator is a fully implicit, fully compositional, finite-difference model.
5.	CMG.	ISCOM model.	ISCOM (Rubbin and Buchanan, 1985) is a fully implicit four-phase (oil, water, gas, and solid) multicomponent finite difference thermal simulator.
6.	Societe Nationale Elf Aquitaine.	IMPES	Elf's model (Corre et al., 1984) is based on the water component, and energy conservation equations.

TABLE 6 FEATURES OF SPE-CSP 5

	Participants	Method/Simulator used	Computer used	Comment
1.	Arco	IMPES or fully implicit	CRAY X/MP	The Arco miscible flood reservoir simulator is based on a limited-compositional formulation (Bolling, 1987)). This simulator is a modified version of SSI's COMP II (Coats, 1979).
2.	British Petroleum (BP).	same	same	same
3.	CMG.	Adaptive-implicit compositional model	Honeywell Multics DPS8/7	For the four-component cases CMG's IMEX, four-component, adaptive-implicit, black-oil model was used with pseudo-miscible option. A semi-analytical approach was used to decouple the flow equations from the flash equations.
4.	Chevron.	Fully implicit	CRAY X/MP	The Chevron miscible flood simulator ("four component simulator") is a fully implicit three-component based on the concepts outlined by Todd and Longstaff, 1972.
5.	Energy Resource Consultants Limited (ERC)	PORES black-oil simulator	NORSK DATA ND 570/CX	same as in Table 2 for black-oil simulator
6.	Reservoir Simulation Research Corp (RSRC)	IMPES	CRAY X/MP	RSR incorporated an IMPES-type equation-of-state compositional model for the simulations.
7.	Todd, Dietrich, and Chase, Inc. (TDC)	Multiflood simulator (Chase and Todd, 1984)	CRAY 1S	This simulator has been designed to reproduce the effects of major mass transfer and phase transport phenomena known to be associated with the miscible flood process with particular emphasis on CO_2 enhanced oil recovery.

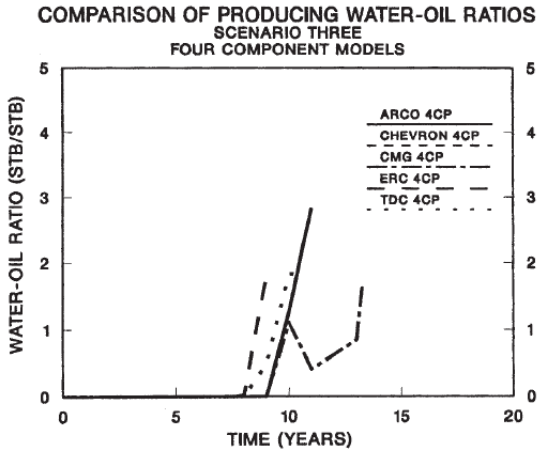

FIG. 2 SCENARIO THREE: COMPARISON OF PRODUCING WATER/OIL RATIOS FOR FOUR COMPONENT MODELS (Killough and Kossack, 1987)

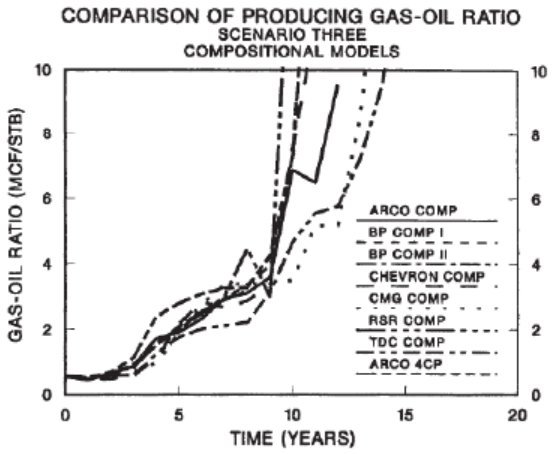

FIG. 3 SCENARIO THREE: COMPARISON OF PRODUCING GAS/ OIL RATIOS OF COMPOSITIONAL MODELS (Killough and Kossack, 1987)

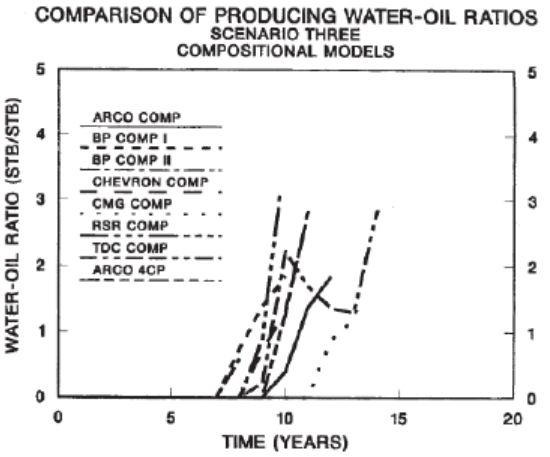

FIG. 4 SCENARIO THREE: COMPARISONS OF PRODUCING WATER/OIL RATIOS FOR COMPOSITIONAL MODELS (Killough and Kossack, 1987)

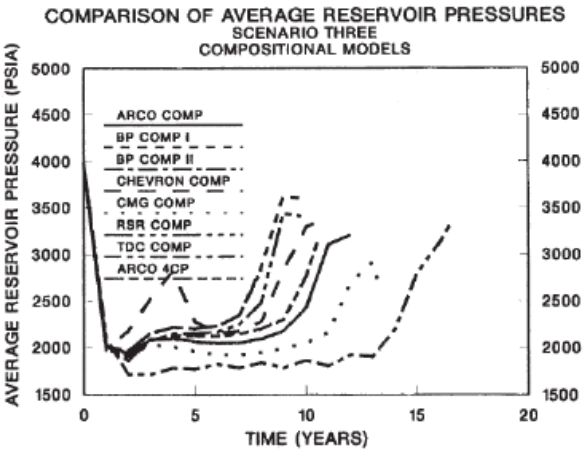

FIG. 5 SCENARIO THREE: COMPARISON OF AVERAGE PORE VOLUME WEIGHTED PRESSURE FOR COMPOSITIONAL MODELS (Killough and Kossack, 1987)

Fifth SPE-CSP

The fifth CSP presented the results of comparisons between both four-component miscible flood simulators and fully compositional reservoir simulation models from seven different participants (shown in Table 6) for a series of three test cases (Killough and Kossack, 1987). These cases varied from scenarios dominated by immiscible conditions to scenarios in which minimum miscibility pressures were maintained or exceeded throughout the simulations. Three injection and production scenarios were designed to test the abilities of the four–component and compositional models to simulate the WAG injection process into a volatile oil reservoir. The problem was not much practical, however, both the coarse grid and the extremely light reservoir oil were chosen to allow the problem to be simulated in a reasonable amount of computational time with a fully compositional simulator. Agreement between the models was good for the first two scenarios. However, relative permeability, pressure and compositional results for scenario three showed a substantial deviation among the participants. For instance, Figure 2 indicates that the main reason for the differences may be a minor difference in relative permeability treatment at the producer for the CMG case. Both GOR's and WOR's began increasing at the same time for all models except Chevron model. The WOR climbed somewhat more slowly for the CMG model in turn causing the GOR maximum to be reached well after the other models. As seen in Figure 3, GOR for all models began to rise above 2 MCF/STB at approximately the same time; however, GOR for the CMG and TDC models appeared to increase at a slower rate than the other models. This may be the result of the use of different injectivity treatments by the participants. Figure 4 shows that WOR behavior for all models was similar with breakthrough occurring at about the same time. Average reservoir pressure results for the compositional models were again erratic as it can be seen from Figure 5. For the test case in which reservoir pressure was maintained above the minimum miscibility pressure, agreement between four–component simulators, with the assumption of complete mixing of solvent and oil, and compositional simulators was excellent based on cumulative oil production as a function of cumulative water injection. For cases in which immiscible conditions dominated, the four-component models tended to be downbeat compared to fully compositional models because condensable liquids were not considered to be carried in the gasesous phase in the four – component simulations. Relative permeability treatment, especially near the injection well, pondered to dominating the timing of recovery and injection breakthrough.

Sixth SPE-CSP

As the simulation of naturally fractured petroleum reservoirs was in great demand, sixth CSP (Firoozabadi and Thomas, 1990) was designed to illustrate some aspects of the physics of multiphase flow in fractured reservoirs and modeling techniques to account for capillary and gravity forces. The approach to the solution of the problems has been limited to dual-porosity models. Two problems were selected to compare fractured reservoir models: a single-block example and a more complicated cross-sectional example developed to simulate depletion, gas-injection, and water-injection as well. The influence of fracture capillary pressure on reservoir performance has been addressed by cases with zero

and nonzero gas/oil capillary pressure in the fractures. Ten organizations (shown in Table 7) participated in this project. The comparison of solutions from various participants indicated a noticeable difference in the results for some examples. There were large differences of results for the case of nonzero fracture capillary pressure. Different formulations for matrix/fracture exchange were considered to be the main reason for this disagreement. This project conveyed an important message that the difference between the cases with zero and nonzero fracture capillary pressure indicated the future need of development of the physics and numerical modeling of naturally fracture petroleum reservoir.

TABLE 7 FEATURES OF SPE-CSP 6

	Participants	Method/Simulator used	Comment
1.	Chevron Oil Field Research Co.	Naturally fractured reservoir simulator (NFRS).	This simulator is based on the methodology outlined in Chen et. al., 1987.
2.	CMG	IMEX	This is both a single-porosity and a dual-porosity/dual permeability, four component, adaptive-implicit reservoir simulator. For the dual porosity option, IMEX allows the discretization of the matrix blocks into subblocks either in the nested format (Pruess and Narasimhan, 1985), for the representation of transient effects, or in the layer format, for the representation of gravity effect (Gillman, 1986).
3.	Dancomp A/S	DANCOMP/RISO Simulator.	This is a three phase, 3D, isothermal model that can be run in either black-oil or compositional models with a dual-porosity/ dual permeability option.
4.	Exploration Consultants Ltd. (ECL)	ECLIPSE	This is a fully implicit program and reinjects a fraction of the phase production or reservoir voidage from the current time step to model pressure-maintenance schemes. This approach has been used in the gas-injection runs rather than reinjecting gas from the previous timestep.
5.	FRANLAB	FRAGOR	This is a three phase, 3D, black-oil, pseudo- and fully compositional simulator with a dual-porosity/dual permeability model (Quandale and Sabithier,1988).
6.	Japan Oil Engineering Co. (JOE)	Fully implicit	JOE and Japan Natl. Oil Corp. jointly developed this simulator. This uses a finite difference spatial discretization in which flow terms are weighted upstream and applies a fully implicit backward Euler method for the time discretization.
7.	Marathon Oil Co.	Fractured Simulator	This is a fully implicit, three phase, 3D model. Matrix/Fracture fluid-transfer functions for each phase are based on the transmisissibilities reported by Gillman and Kazemi, 1983.
8.	Philips Petroleum Co.	Fully implicit	This is a fully implicit, 3D, three-phase, single or dual-porosity model.
9.	Simulation and Modeling Consultancy Ltd. (SMC)	GENESYS	SMC's three-phase, 3D GENESYS simulator is designed to model both fractured and unfractured petroleum reservoirs (Sonier and Eymard, 1987).
10.	SSI	SIMBEST II	This simulator was designed to expand traditional black-oil simulation to include dual-porosity and pseudocompositional behavior. This allows automatic accounting of phase pressure differences between the matrix and fracture when the matrix is subjected to capillary equilibrium and the fracture is in vertical equilibrium.

TABLE 8 FEATURES OF SPE-CSP 7

	Participants	Method/Simulator used	Comment
1.	ARTEP (Research association of Institut Francais du Petrole, Elf Aquitaine, Total-CFP and Gas de France)	Sigma-Core	This is three-phase, 3D black-oil and compositional model.
2.	Chevron oil Field Research Company	Fully implicit black-oil simulator	This simulator is with Cartesian local grid capability (Wasserman, 1987).
3.	CMG	IMEX	This is an adaptive implicit, three-phase, black-oil simulator with pseudo-miscible options (Fung et al., 1989).
4.	ECL Petroleum technologies (ECL)	Eclipse 100 and Eclipse 200	These are fully implicit, general purpose black-oil simulator with gas condensate.

5.	Robertson ERC Ltd (ERC)	TIGRESS (The Integrated Geophysics Reservoir Engineering Software System)	This is an integrated software system which includes application modules for geophysics, geology, petrophysics, mapping, reservoir engineering, reservoir simulation and economics.
6.	HOT Engineering (HOT)	SURE	This is a general non-isothermal compositional model which is formulated for any number of phases and components while the input data and results remain in well-known black-oil format.
7.	Integrated technologies (INTECH)	VIP-ENCORE	This is a three-phase, 3D, vectorized, fully implicit (or IMPES) simulator in which internally the hydrocarbon fluids are handled compositionally.
8.	Japan National Oil corporation (JNOC)	Fully implicit black-oil model	This coupled a fully implicit black-oil model to a model for multi-phase flow in pipes to include wellbore hydraulics in the calculations.
9.	Marathon Oil Company	Fully implicit	This is based on Gillman and Kazemi, 1983.
10.	Philips Petroleum Company		This is a general purpose three dimensional, three-phase reservoir model that can be used to simulate vertical, inclined and horizontal wells.
11.	RSRC		A detailed description of the simulator used in this study is presented by Young, 1988.
12.	Shell development Co.	Black-Oil	The simulator used was the implicit black-oil version of Shell's multipurpose isothermal reservoir simulator.
13.	Stanford University		The simulator used is a three-dimensional, three-phase research simulator with local grid refinement, hybrid grid and domain decomposition options.
14.	TDC	BLOS	This is a standard 3D, three-phase, three-component, IMPES, finite difference based simulator.

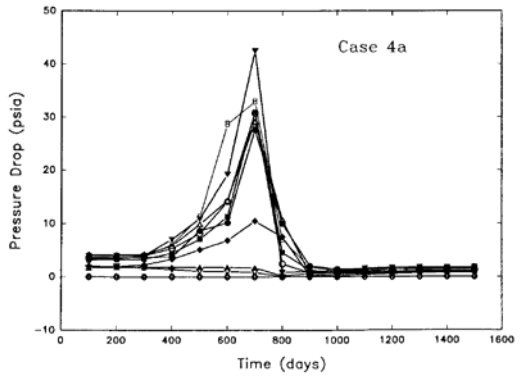

FIG. 6 TOTAL PRESSURE DROP ALONG WELLBORE FOR CASE 4a (Nghiem et al., 1991)

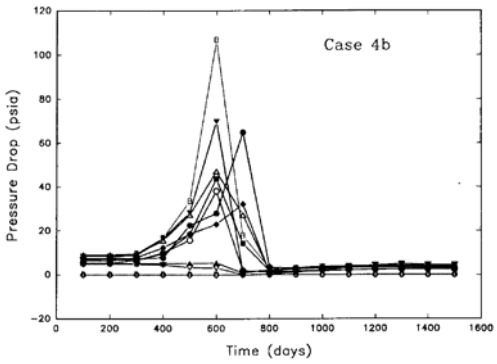

FIG. 7 TOTAL PRESSURE DROP ALONG WELLBORE FOR CASE 4b (Nghiem et al., 1991)

Seventh SPE-CSP

Because of improved drilling technology, and the increased efficiency and economy of oil recovery operations, interest in horizontal wells rapidly accelerated. Seventh CSP (Ngheim et al., 1991) presented a problem which dealt with the effect of horizontal well lengths and rates on the recovery, in which fourteen organizations participated. These are illustrated in Table 8. The problem designed with oil recovery by bottom water drive in a thin reservoir where coning was concerned. Black-oil fluid properties and relative permeabilities from the second CSP were used. However, reservoir and capillary pressure values were different. A variety of methods was used by the participants to model the inflow into the horizontal wells ranging from the use of productivity indices to grid refinement. A multitude of techniques was also used to calculate wellbore hydraulics while a few contributors were selected to represent the wellbore by a constant-pressure line sink. All participants consistently predicted a decrease in the coning behavior with an increase in well length. In comparisons, there were substantial variations in peak pressure drop among the participants. These are shown in Figures 6 and 7 as an example. The figures show the predicted pressure drop along the well bore. The pressure drop increased with increasing free gas flow rates. There were sizeable variations in the peak pressure drop predicted. The truncation errors, convergence criteria, time steps taken and implicit/ explicit formulation were possible grounds behind the differences. The effect of wellbore hydraulics could not be understood from the simulation results.

Eighth SPE-CSP

The eighth CSP (Quandalle, 1993) was designed with the aim to compare flexible gridding techniques. This was performed by five participants and the problem posed was a 3D simulation of oil production associated with gas injection in a four layer reservoir. Organizations participated are shown in Table 9, who were asked to provide two sets of results with the same simulator, the first corresponding to a simulation run with a regular Cartesian grid 10x10x4, and a second set corresponding to a simulation run with a flexible grid optimized to have as few grid cells as possible. This CSP was also an academic exercise of flexible gridding techniques. The major conclusion of this study was that the flexible gridding schemes are reliable and they can allow a significant computer time saving for the reservoir simulation. In a case oil displacement by a much more mobile gas, all participants could reduce the total number of grid nodes by a factor of four or more with flexible gridding while simulation results could keep close to those obtained with regular gridding technique.

Ninth SPE-CSP

The ninth CSP (Killough, 1995) was designed to reexamine of black-oil simulation based on a model of moderate size (9000 cells) and with a high degree of heterogeneity provided by a geostatistically-based permeability field. Nine organizations participated in this project reported in Table 10 were asked to report results for the simulation several ways. The primary data collected were the field total producing rates for oil, gas, and water. The variation of field oil rates was within 9% of the mean value for all parties, slightly larger for the field gas rates than that in the case of the oil rates with the maximum deviation of 11% of the mean value. The water rate for all participants varied considerably. Maximum deviation after about 100 days was on the order of 20%. The main reason for this probably laid in the treatment of relative permeabilities and capillary pressures. As shown in Figure 8, near the end of the simulation, the variation in water saturation was about 25% among the participants. Variations may also has been due to the amount of water injection allowed due to bottom hole pressure constraint. Injection rates varied considerably due to conditions in the aquifer (i.e., use of 100% water saturation) as it can be seen in Figure 9. In this CSP, the participants also supplied data concerning the number of time steps, non-linear iterations and CPU time associated with the model simulations.

TABLE 9 FEATURES OF SPE-CSP 8

	Participants	Method/Simulator used	Comment
1.	CMG	STARS	This is an adaptive-implicit, multicomponent, dual-porosity, advanced process simulator capable of handling isothermal and thermal processes.
2.	INTERA Information Technologies(INT)	ECLIPSE 100/200	same as in Table 7 for ECLIPSE
3.	Beicip-franlab (B-F)	FRAGOR	This is a multipurpose reservoir simulator which includes black-oil and multicomponent, single and dual porosity capabilities (Quandalle and Sabathier, 1987).
4.	SMC	GENESYS	same as in Table 7 for SMC
5.	Stanford University	META	This is the simulator used was developed by Nacul (1991) and Nacul and Aziz (1991). This is a fully implicit three-dimensional black-oil simulator with adaptive implicit and IMPES options.

TABLE 10 FEATURES OF SPE-CSP 9

	Method/simulator used	Comment
1.	TechSIM simulator used by AEA Technology	This simulator uses a generalized compositional model and includes option for black oil, miscible flood and equation of state compositional simulation.
2.	ARCO	This is a black-oil simulator employs IMPES and fully implicit techniques for time step discretizations.
3.	CMG	same as in Table 8
4.	INTERA Information Technologies	same as in Table 9
5.	SENSOR	This is a three dimensional, three phase reservoir simulation model for black-oil and compositional applications (Coats, 1995).
6.	SSI	same as in Table 7
7.	Fina	same as SSI
8.	TIGRESS	same as in Table 7
9.	Desktop-VIP used by Western Atlas Software	This is a multicomponent, 3D, three phase reservoir simulator which contains a number of modules sharing a common compositional formulation.

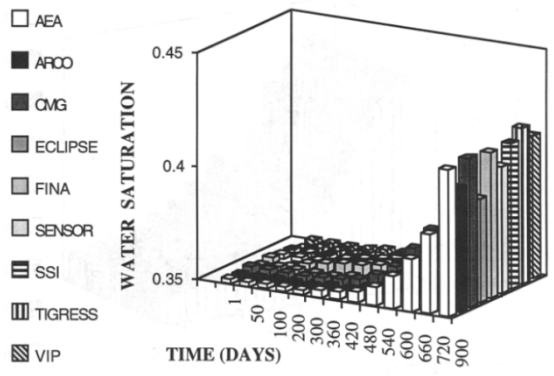

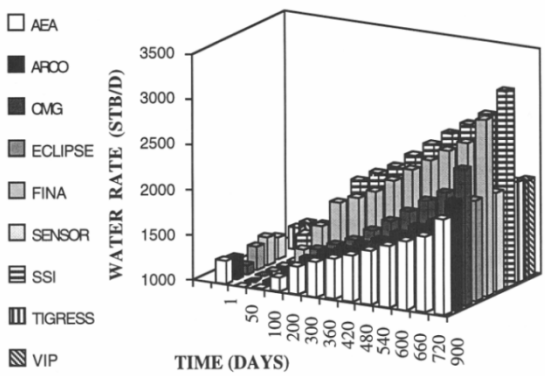

FIG. 8 COMPARISON OF WATER SATURATIONS (Killough, 1995) FIG. 9 COMPARISON OF WATER INJECTION RATES (Killough, 1995)

TABLE 11 FEATURES OF SPE-CSP 10

	Participants	Method/Simulator used	Comment
1.	Chevron	CHEARS	Chevron used the parallel version and the serial version for the fine grid model, and the serial version for the scaled-up model.
2.	Coats Engineering Inc.	SENSOR	same as in Table 9
3.	GeoQuest	ECLIPSE 100 and FRONTSIM	FRONTSIM is a streamline simulator to check the accuracy of the upscaling (Christie and Blunt, 2001).
4.	Landmark	VIP	same as in Table 9 for Desktop-VIP
5.	Philips Petroleum	SENSOR	same as in Table 8
6.	Roxar	Nextwell and	The simulation results presented were generated using Roxar's Black-Oil, Implicit Simulator, Nextwell. The upscaled grid properties were generated using Roxar's Geological Modeling sofawre, RMS, in particular the RMSsimgrid option.
7.	Streamsim	RMSsimgrin	Simulations were run using 3DSL, a streamline based simulator designed by Batcky et. al., 1997.
8.	TotalFinaElf	ECLIPSE	Same as in Table 7 for ECLIPSE
9. Wales	University of New South		The University of New South Wales submitted results for model 1 only using CMG's IMEX simulator.

TABLE 12 SUMMARY OF AVAILABLE BENCHMARK TIMES FOR SPE 10 SOLUTIONS

Reference	Time	Notes
(Hammersley and Ponting, 2008)	328 Minutes	128 steps, uses algebraic multigrid
(Gong, 2011)	4.5 hours	General-purpose Research Simulator (GPRS), 1 CPU
(Gong, 2011)	5 hours	Eclipse on 8 CPUs, though no explanation of cores versus CPU
(Esler et al., 2012)	27 Minutes	In-house simulator; Uses operator split, pressures solved with 20-day steps, saturation propagated with 1000's of independent explicit steps; uses Tesla GPU, and single precision for saturations
(Esler et al., 2012)	24+ Hours	In-house simulator; Uses operator split, pressures solved with 20-day steps, saturation propagated with 1000's of independent explicit steps; uses sequential solver, single CPU
(Kwok, 2007)	16558 Seconds	53 steps
(Gratien et al., 2007)	7169 (1 CPU) /620 (64 CPU) seconds	2 processes on each CPU
(Natvigand et al., 2009)	170 seconds	Parallel streamline simulator, "highly optimized commercial simulator," 13 time steps

Tenth SPE-CSP

Upscaling techniques used in the tenth CSP in series performed by nine participants were investigated by (Christie and Blunt, 2001). Two problems were chosen, the first of which was a small 2D gas-injection problem where the fine grid could be computed easily and both upscaling and pseudoization method could be used while the other was a waterflood of a large geostatistical model where (though not impossible) the true fine-grid solution is difficult to compute. Name of participants are shown in Table 11. For the first problem, the permeability distribution was a correlated geostatistically field. The fluids were assumed to be incompressible and immiscible. Capillary pressure was assumed to be negligible. Gas was injected from an injector located at the left of the model and dead oil was produced from a well on the right of the model. This was a relatively easy problem, and all participants were succeeded to obtain coarse

grid solutions that agreed well with their own fine grid results. Mostly, these results were obtained by a history matching process to compute cross grid relative permeabilities. Roxar showed that it was also possible to obtain good results using only single phase upscaling and local grid refinement, and Coats showed that it was possible to obtain a good match with a homogeneous permeability and the original rock curves on a coarse grid. For the second problem, the model had a sufficiently fine grid to make use of any method that relied on having the full fine grid solution almost impossible**.** The model had a simple geometry, with no top structure or faults. This was to provide maximum flexibility in selection of upscaled grids. For this model, the fine grid streamlines simulations submitted by Geoquest and Streamsim were in good agreement with the fine grid finite difference solutions submitted by Landmark and chevron. In addition, the intermediate grid solutions submitted by Philips and Coats were close to the full fine grid solutions, except for the field average pressure. In this project, it was found that going to a coarse grid (of the size that could be used if the model represented a pattern element of a full field model) induced large errors. Interestingly, there was little difference between the 20x44x17 and the 30x55x17 predictions, but both were some way away from the fine grid solution. At the grid size submitted, there was as much variation in results due to the choice of upscaling approaches. The results submitted by the participants also showed significant differences irrespective of pseudo-based and the upscaling techniques. From this study, it was concluded that the best single phase method is flow-based upscaling using no-flow boundary conditions.

It has been twelve years since the last (tenth) CSP was conducted. By this time, there has been tremendous improvement in computational power; numerous state-of-the-art models, simulators are developed. Table 12 provides a summary of reported timings for solution of the full SPE 10 problem from Refs (Elser et al., 2012; Gong, 2011; Gratien et al., 2007; Hammersley and Ponting, 2008; Kwok, 2007; Natvigand et al., 2009). After 2001, the single-core (sequential, non-parallel) floating point speed is improving each year by 21-52% as reported by Standard Performance Evaluation Corporation (www.spec.org). On the other hand, moving sequential simulators to parallel computations more speed-up can be achieved. Table 12 shows that through parallel computations the SPE-10 problem can be solved even within couple of seconds!

Concluding Remarks

Validation of reservoir simulators for complex recovery processes is a particularly difficult problem because analytical solutions are available under only a few limiting conditions. While good agreement between the results from different simulators for the same problem necessarily does not ensure any valid result, and a lack of agreement does give cause for some concern. Such comparisons can also be useful in the development of new models and in optimizing the performance of existing reservoir simulators. The results presented in CSPs are very important from practical point of view although there were some significant differences in many cases. However, the problems and results presented in CSPs are of value in enhancing the state of reservoir simulation technology.

ACKNOWLEDGEMENT

We thank SPE to give permission to reprint the graphs presented in this article. The work was conducted with the support of the Reservoir Simulation Joint Industry Project, a consortium of operating and service companies for Petroleum and Geosystems Engineering at The University of Texas in Austin.

REFERENCES

Aziz, K., Ramesh, B., and P. T. Woo. "Fourth SPE comparative Solution Project: A Comparison of Steam Injection Simulators." SPE 13510, 8th SPE Symposium on Reservoir Simulation, Dallas, 1985.

Bansal, P. P., Harper, J. L., McDonald, A. E., Moreland, E, E., Odeh, A, S., and R. H. Trimble. "A Strongly Coupled Fully Implicit, Three-Dimensional, Three-Phase Reservoir Simulator." paper SPE 8329 presented at the SPE 54th Annual Technical Conference and Exhibition, Las Vegas, Sept 23-26, 1979.

Batycky, R. P., Blunt, M. J., and M. R. Thiele. "A 3D Field Scale Streamaline Based Reservoir Simulator." SPERE Nov (1997): 246-254.

Bolling, J. D., "Development and Application of a Limited-Compositional Miscible Flood Simulator." SPE 15998, Ninth SPE Symposium on Reservoir Simulation, Feb 1-4, 1987.

Chapplear, J. E., and W. Rogers. "Some Practical Considerations in the Construction of a Semi-Implicit Simulator." SPEJ 14 (1974): 216-220.

Chen, W. H., Wasserman, M. L., and R. E. Fitzmaris. "A Thermal Simulator for Naturally Fractured Reservoirs." SPE 16008, SPE Symposium on Reservoir Simulation, San Antonio, Feb 1-4, 1987.

Cheshire, I. M., Appleyard, J. R., and D. Banks. "An Efficient Fully Implicit Simulator." Paper 179 European Offshore petroleum Conference, London, Oct. 21-24, 1980.

Christie, M. A., and M. J. Blunt. "Tenth SPE Comparative Solution Project: A Comparison of Upscaling Techniques." SPE 66599, SPE Reservoir Simulation Symposium, Houston, Feb 11-14, 2001.

Coats, K. H. "An Equation-of-State Compositional Model." SPE 8284 presented 54th Annual Fall Conference and Exhibition of SPE, AIME, Las Vegas, Sep 23-26, 1979.

Coats, K. H., and M. D. Modine. "A Consistent Method of Calculating Transmissibilities in Nine-Point Difference Equations." SPE 12248, SPE Reservoir Simulation Symposium, San Francisco, Nov 15-18, 1983.

Coats, K. H., and A. B. Ramesh. "Effects of Grid Type and Difference Scheme on Pattern Steamflood Simulation Results." JPT May (1986): 557-569.

Coats, K. H., Thomas, L. K., and R. G. Pierson. "Compositional and Black-Oil Reservoir Simulation." SPE 29111, 12th SPE Symposium on Reservoir Simulation, San Antonio, Feb 12-15, 1995.

Corre, B., Eymard, R., and L. Quettier. "Application of a Thermal Simulator to Field Cases." SPE 13221, Annual Technical Conference and Exhibition, Houston, Sept 16-19, 1984.

Chase, C. A., and M. R. Todd. "Numerical Simulation of CO_2 Flood performance." SPEJ Dec (1984): 596-605.

Esler, K. P., Natoli, V., Samardzic, A., Atan, S., and R. Benjamin. "Accelerating reservoir simulation and Algebraic Multigrid with GPUs." GPU Technology Conference, San Jose, CA., 2012.

Firoozabadi, A., and L. K. Thomas. "Sixth SPE Comparitive Solution Project: Dual Porosity Simulators." JPT 42 (1990): 710-715.

Fung, L, S-K., Collins, D, A., and L. Ngheim. An Adaptive-Implicit Switching Criterion Based on Numerical stability Analysis. SPRE 4 (1989): 45-51.

Gillman, J. R. "An Efficient Finite Difference Method for Simulating Phase segregation in matrix Blocks in Double Porosity Reservoirs." SPERE July (1986): 403-413.

Gillman, J., and H. Kazemi. "Improvements in Simulation of naturally Fractured Reservoirs." SPEJ Aug (1983): 675-707.

Gong, B. "A general purpose reservoir simulator (GPRS) for numerical simulation of CO_2 sequestration." China Australia Geological Storage of CO_2 (CAGS) Workshop 3, Changcuan, China, July 11-15,2011.

Gratien, J. M., Guingon, T., Magras, J, F., Quandalle, P, Q., and O. R. Riocis. "Scalability and Load Balancing Problems in Parallel Reservoir Simulation." SPE 106023, SPE Reservoir Simulation Symposium, The Woodlands, TX, Feb 26-28, 2007.

Hammersley, R. P., and D. K. Ponting. "Solving linear equations in reservoir simulation using Multigrid methods." SPE Russian Oil & Gas Technical Conference and Exhibition, Moscow, Russia, Oct 28-30, 2008.

Kenyon, D. E., and A. Behie. "Third SPE Comparative Solution Project: Gas Cycling of Retrograde Condensate Reservoirs." JPT (1987): 981-997.

Khashan, S. A., Ogbe, D. O., and T. M. Jiang. "Development and Optimization of Parallel Code for Large Scale Petroleum Reservoir Simulation." JCPT 41 (2002): 33-38.

Killough, J., and C. Kossack. "Fifth SPE Comparative Solution Project: Evaluation of Miscible Flood Simulators." SPE 16000 presented at the SPE Symposium on Reservoir Simulation, San Antonio, Feb 1-4, 1987.

Killough, J. "Ninth Comparative Solution Project: A Rexamination of Black Oil Simulator." SPE 29110, 13th SPE Symposium of Reservoir Simulation, San Antonio, Feb 12-15, 1995.

Killough, J, E., and R. Bhogeswara. "Simulation of Compositional Reservoir Phenomena on a Distributed-Memory Parallel Computer." JPT (1991): 1368-1374.

Kwok, W. H. F. "Scalable Linear and Nonlinear Algorithms for Multiphase Flow in Porous Media." PhD Dissertation, Stanford University, CA., 2007.

Lolomari, T., Bratvedt, K., Crane, M., Milliken, W., and J. Tyrie. "The Use of Streamline Simulation in Reservoir Management Methodology and Case Studies." SPE 63157, SPE annual meeting, Dallas, Oct 1-4, Oct 2000.

Nacul, E. C. "Use of Domain decomposition and Local Grid Refinement in Reservoir Simulation." PhD Dissertation,

Stanford University, 1991.

Nacul, E . C., and K. Aziz. "Use of Irregular Grid in Reservoir Simulation." SPE 22886, 66th SPE Technical Conference and Exhibition, Dallas, Oct 6-9, 1991.

Natvigand, J. R., Skaflestad, B., Bratvedtand, F., and K.-A. Lie. "Multiscale Mimetic Solvers for Efficient Streamline Simulation of Fractured Reservoirs." SPE-119132, Reservoir Simulation Symposium, The Woodlands, TX, Feb 2-4, 2009.

Ngheim, L., Collins, D, A., and R. Sharma. "Seventh SPE Comparative Solution Project: Modeling of Horizontal Wells in Reservoir Simulation." SPE 21221, 11th SPE Symposium on Reservoir Simulation, Anaheim, Feb 17-20, 1991.

Nolen, J. S., and P. L. Stanata. "Reservoir Simulation on Vector processing Computers." SPE 9644, SPE Middle East Technical Conference, Bahrain, March 9-12, 1981.

Odeh, A. "Comparison of Solutions to a Three Dimensional Black-Oil Reservoir Simulation Problem." JPT 33 (1981): 13-25.

Price, H. S., and K. H. Coats. "Direct Methods in Reservoir Simulation." SPEJ (1974): 295-308.

Pruess, K., and T. N. Narasimhan. "A Practical Method for Modeling Fluid and Heat Flow in Fractured porous media." SPEJ Feb (1985): 14-26.

Quandale, P., and J. C. Sabithier. "Typical Features of a New Multipurpose Reservoir Simulator." SPERE Nov (1988): 1114-1122.

Quandalle, P. "Eighth SPE Comparative Solution Project: Gridding Techniques in Reservoir Simulation." SPE 25263, Twelfth SPE Symposium on reservoir Simulation, New Orleans, Feb 28-march 3, 1993.

Quandalle, P., and J. C. Sabathier. "Typical Features of a New Multipurpose Reservoir Simulator." SPE 16007, 9th SPE Reservoir Simulation Symposium, San Antonio, Feb 1-4, 1987.

Rubbin, B., and W. L. Buchanan. "A general Purpose Thermal Model." SPEJ, April 1985, 202-214.

Sonier, F., Besset, P., and O. Ombert. "A Numerical Model of Multiphase Flow Around a Well." SPEJ (1973): 311-320.

Sonier, F., and R. Eymard. "A New Simulator for Naturally Fractured Reservoirs." SPE 16006, SPE Symposium on Reservoir Simulation, San Antonio, Feb 1-4, 1987.

Spillete, A. G., Hillestad, J. G., and H. L. Stone. "A High Stability Sequential Solution Approach to Reservoir Simulation." SPE 4542, SPE 48th Annual Meeting, Las Vegas, Sep 30-Oct 3, 1973.

Stanta, P. L., and J. S. Nolen. "Performance Comparisons for Reservoir Simulation Problems on Three Supercomputers." SPE 10640, SPE Symposium on Reservoir Simulation, New Orleans, Feb 1-3, 1982.

Stone, H. L. "Probability model for Estimating Three-Phase Relative Permeability." JPT 249 (1970): 214-218.

Stone, H. L. "Estimation of Three-Phase Relative Permeability and Residual oil Data." Annual Technical Meeting of CIM, Edmonton, Canada, May 8-12, 1973.

Tan, T. B. S., and J. P. Lakeman. "Application of D4 Ordering and Minimization in an Effective Partial Matrix Inverse Iterative Method." SPE 10493, SPE Symposium on Reservoir Simulation, New Orleans, Feb 1-3, 1982.

Thomas, G. W., and D. H. Thurnau. "The mathematical Basis of the Adaptive Implicit method." SPE 10495, SPE Symposium on reservoir Simulation, New Orleans, Feb 1-3, 1982.

Todd, M. R., O'Dell, P. A., and G. J. Hirasaki. "Methods of Increased Accuracy in Numerical Reservoir Simulations." SPEJ Dec (1972): 515-530.

Todd, M. R., and W. J. Longstaff. "The Development, Testing, and Application of a Numerical Simulator for Predicting Miscible Flood Performance." JPT July (1972): 874-882.

Wasserman, M. L. "Local Grid Refinement for Three-Dimensional Simulators." SPE 16013, SPE Symposium on Reservoir simulation, San Antonio, Feb 1-4, 1987.

Weinstein, H. G., Chappelear, J. E., and J. S. Nolen. "Second Comparative Solution Project: A Three Phase Coning Study." JPT 38 (1986): 345 – 353.

Yanosik, J. L., and T. A. McCraken. "A nine-Point, Finite Difference Reservoir Simulator for Realistic Prediction of Adverse Mobility Ratio Displacements." SPEJ, (1979): 253-262.

Young, L. C. "Full Field Compositional Model on vector processors." SPE 17803, SPE Rockey Mountain Regional Meeting, Casper, May 11-13, 1988.

Akand Islam is a postdoctoral fellow at The Center for Petroleum and Geosystems Engineering, The University of Texas in Austin. His research mainly focuses on petroleum

reservoir simulation, especially developing computationally efficient phase equilibrium and thermophysical modeling. He obtained his PhD in Chemical Engineering from The University of Alabama. He has published several papers in scientific journals.

Kamy Sepehrnoori holds the W. A. (Monty) Moncrief Centennial Chair in Petroleum Engineering at The University of Texas in Austin. His research areas are focused on computational methods, reservoir simulation development and application, EOR modeling, naturally fractured reservoirs, inverse problems, and unconventional resources. He obtained his PhD in Petroleum Engineering from The University of Texas at Austin.

Journal of Petroleum Science Research (JPSR) Volume 2 Issue 4, October 2013 www.jpsr.org
doi: 10.14355/jpsr.2013.0204.05

Numerical Study on the Gas-Liquid Two Phase Flow in Pipeline Commissioning

Xinyu Zhang[1], Bo Yu[*1], Dongping Qiu[2], Xu Sun[2]

National Engineering Laboratory for Pipeline Safety/Beijing Key Laboratory of Urban Oil and Gas Distribution Technology, China University of Petroleum
Fuxue Road 18#, Changping District, Beijing, 102249, China
Sinopec Pipeline Storage & Transportation (Branch) Company
Zhaishan New Residential Quarters, Quanshan District, Xuzhou, 221008, China

Corresponding Author: yubobox@vip.163.com

Abstract

Pipeline commissioning is a gas-liquid two phase flow process. In the hilly area, the complex flow status in pipeline may threaten the safety of the commissioning process. This paper developes a novel numerical technology to simulate the hydraulic process of pipeline commissioning. Several alternative modules are established, focused on which physical and mathematical models are established respectively to describe its flow status and corresponding pressure drop. With the aid of recognition technology and regulation and control technology, connection of these pipe sections can be performed to represent the actual pipeline and thus realizing the simulation of pipeline commissioning process.

Keywords

Pipeline Commissioning; Gas-liquid Two Phase Flow; Numerical Method; Simplified Model

Introduction

In recent years, with the rapid development of pipeline construction, the commissioning process has attracted more and more attention. Among all the commissioning methods, direct commissioning has become a mainstream method due to its time efficiency and low cost.(Nan Zhang et al. 2008, Zengqiang Zhang 2004, Shaoqing Li 2002, Guotai Shao et al. 2005)

In the process of direct commissioning, before the oil is filled into pipeline, a series of preparation work, such as hydraulic test and pipeline internal cleaning has to be performed. During the cleaning process, it is impossible to remove all water remained from hydraulic test. Therefore, gas-liquid two phase flow may occur in the subsequent pipeline operation. In the engineering practice, the terrain of the area where pipelines lays can be complex while the hydraulic characteristics, such as flow pattern, pressure drop and liquid holdup of pipeline in hilly area greatly differ from those of horizontal pipe. Thus, it is necessary to study the gas-liquid two phase flow in the commissioning processes of pipelines, especially on hilly areas.

In the commissioning process, field staffs most concern about the flow pattern and corresponding pressure drop in the pipeline. For the flow pattern, there have been some mature technologies, such as VOF (C.W. Hirt et al. 1981) method. However, very fine grid is indispensible in these methods which lead to relatively long calculation time and thus only fitting to the problem of small scale. As to the problem, this paper regards length of the pipeline that generally can reach hundreds of kilometers. If this kind of method is adopted, the calculation time and memory required are unacceptable. On the other hand, in the engineering practice, only the macro information such as pipeline inlet pressure and flow friction, rather than details such as breaking and coalescence behavior of bubbles is concerned. Thus, based on the constriction of computation condition and the requirement of engineering application, the numerical simulation of commissioning process aims at obtaining macro information of engineering guiding significance. Jing Gong et al. (1995) analyzed steady and transient flow characteristics of the long slop pipelines with the existence of partial flow based on fluid mechanics principles. Nan Zhang (2009) performed quasi-steady simulation of gas-liquid stratified flow in a declined pipe under constant flow rate based on non-wave model, drift-flow model and homogeneous flow model respectively. Boyi Liang (2011) used CFD software OLGA to establish a commissioning model under various conditions for comparison. However, to the best knowledge of the present authors, researches with the aim at commissioning process of hilly

pipeline are far from mature. Focused on this problem, this paper develops a novel simulation technology.

Physical and Mathematical Model

In the commissioning process, area terrain is the principal factor influencing its hydraulic process. Previous numerical experiments in which the charge-in process of local pipe sections was simulated indicated that different characteristics are shown when water front flows pipeline of different terrains. Therefore, it is necessary to establish models for the pipelines of different terrains respectively. Actual pipeline can be represented by the combination and connection of these basic pipe section modules.

Establishment of Basic Modules

To avoid the unnecessary troubles in programming, the interaction of modules should be as few as possible. Thus, the modules should be serializable, that is, the inlet boundary of every module should be full pipe flow-in. Based on this principle, the following 9 basic modules are determined.

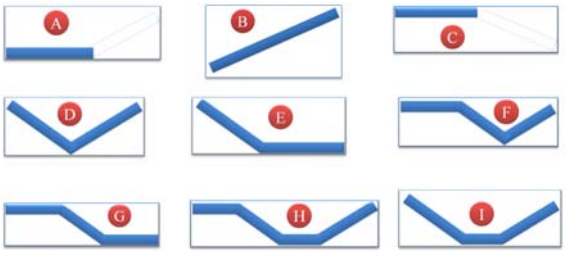

FIG. 1 SCHEMATIC OF BASIC MODULES

For the sake of brevity, only the mathematical model of D-type, F-type, H-type and I-type will be given concretely. In this kind of modules, huge stagnant air pockets may form in the declined pipe section. Once formation, these air pockets are continuously compressed during the commission process. Pressure of the air pocket may reach a high value and lead to local overpressure which is dangerous to the commissioning process. Thus, this kind of modules should be paid most attention. Due to the complexity of its terrain, the commissioning process of pipeline can be divided into several phases, among which the ones after air pockets forms are most critical and thus being emphatically discussed in the following.

Firstly, critical cleaning velocity is adopted to determine whether the air pocket would form or not. Only when the velocity of full pipe water front becomes greater than this velocity, would the stagnant air pocket form. Its value can be determined as Eq(1) shows.

$$v_c = \varsigma\sqrt{gD\sin\theta} \tag{1}$$

where g is gravity acceleration; D is pipeline diameter; θ is inclination of declined pipe section; ς is empirical coefficient, which should be determined by numerical experiment.

1) Situation Where Stagnant Air Pocket Would Form

Hydraulic parameters of air pocket meet the following relationship.

$$p_a V_a = const_1 \tag{2}$$

where p_a and V_a represent the pressure and volume of the air pocket, respectively; $const_1$ is determined by the initial volume of the air pocket.

Hydraulic parameters of the liquid slug at the bottom of the module meet the following relationship.

$$\left(p_a - p_e\right)A - L_s \cdot \pi D \cdot \tau - \rho A g\left(h_2 - h_1\right) = 0 \tag{3}$$

where A is pipe section area; τ is friction force per unit area; p_e is pressure at the pipeline end; L_s is length of the liquid slug; h_1 and h_2 are liquid height of the closed side and open side respectively.

Meanwhile, geometrical parameters should satisfy the following relationship.

$$\frac{\partial h_1}{\partial t}A\left(1-\phi_a\right) + \frac{\partial h_2}{\partial t}A = Q \tag{4}$$

where Q is volume flow rate; ϕ_a is liquid holdup in the declined pipe section.

With Eq(2), Eq(3) and Eq(4), combining the following geometrical relationship, flow status in the pipeline can be solved.

$$V_a = \left(L_{dec} - \frac{h_1}{\sin\theta_1}\right)A\left(1-\phi_a\right) \tag{5}$$

$$L_s = \frac{h_1}{\sin\theta_1} + \frac{h_2}{\sin\theta_2} + L_{hor} \tag{6}$$

where L_{dec} and L_{hor} are length of declined pipe section and bottom horizontal pipe section respectively. As to D-type and F-type pipe section, $L_{hor} = 0$.

2) Situation Where Air Pocket Would Not Form

In this situation, head of the air pocket flows down with liquid flow while gas of the air pocket is continuously discharged at the bottom. Firstly, slip ratio γ of the air pocket head is defined as following

$$\gamma = \frac{v_h}{v_f} \tag{7}$$

where v_h is the velocity of bubble head; v_f is the full pipe flow velocity; γ can be determined by numerical experiment.

Hydraulic parameters of air pocket meet the following relationship.

$$\frac{p_a V_a}{m_a} = const_2 \tag{8}$$

where m_a is air pocket mass; $const_2$ is determined by the initial state of air pocket.

Air pocket volume is determined by the following equation.

$$V_a^n = V_a^{n-1} - v_h^{n-1} A(1-\phi_a) \cdot \Delta t \tag{9}$$

What needs to be notified is that coefficient γ is relevant to air pocket pressure and thus time-dependent.

Air pocket mass is determined by the following equation.

$$m_a^n = m_a^{n-1} - \rho_a^{n-1}\left(V_a^n - V_a^{n-1}\right) \tag{10}$$

where ρ_a^{n-1}, the gas density in the air pocket at last step, can be determined by the following equation.

$$\rho_a^{n-1} = \frac{m_a^{n-1}}{V_a^{n-1}} \tag{11}$$

Solving the above equations simultaneously, the simulation of hydraulic status of this situation can be performed.

Connection of the Modules

In Section 2.1, physical and mathematical models of the modules are introduced. In the following, the approach to perform the connection of these 'basic elements' to represent the actual pipeline will be discussed. To improve the versatility, the connection approach should solve the following problems.

(1)Automatic recognition can be performed with pipeline route profile to determine the connection sequence of referred modules;

(2)A module may occur repeatedly;

(3)As to the modules where air pocket may form, such as D-type and H-type, their hydraulic status is independent of that of the subsequent pipe sections.

Focused on these problems, a program flow is designed. For convenience, after the division of the whole pipeline by recognition module, along the direction from inlet to outlet, the pipe sections are named 1#, 2#, 3# and so on.

Due to the interaction between pipe sections, every pipe section should be incorporated in the whole simulation process other than simulated respectively and then composited. Therefore, every module is designed to be of the following structure: called each time, the simulation is performed forward for a single time step. By this, the modules can be serialized and timely perform the data transmission and feedback.

During the simulation process, the following details are noteworthy. Firstly, calculation of a module should be just started when full pipe flow water front reaches its inlet. Thus, the obtained hydraulic status of every module should be fed back to the regulation and control module to judge which module should be started in the next time step. Secondly, since the call of every modules is not continuous, the obtained data recording the hydraulic status should be temporarily stored into a data storage. This data would be used as calculation condition and input to the 'calculator' in the next time step when this module is called again. Meanwhile, every module may appear multiple times in a pipeline and thus multiple data storage should be set up to store the corresponding data obtained in different locations of the same module to avoid the confusion in data transmission.

For the modules where air pockets may form, their hydraulic status is dependent on that of subsequent pipe sections. Thus, their locations should be recorded so that the hydraulic status of subsequent pipe sections can be timely fed back to corresponding pipe sections in the regulation and control module.

With this approach, the above-mentioned requirement can be satisfied. And the basic modules can be correctly connected.

Example and Analysis

Hereinbefore, the technology this paper develops to simulate the commissioning process of pipeline on the area of complex terrain is described. Since the study of this technology is still at the beginning, only a simplified pipeline is considered and analyzed here, whose pipeline route profile is as shown in Fig. 2 while pipeline diameter is 0.813 m and charge-in water flow rate is 1500 kg/s.

In this example, the pipeline can be divided into 4 sections which correspond to the B-type, D-type, A-type and B-type, respectively. Based on this,

simulation of its commissioning process is performed. The obtained changing trend of pressure drop is as Fig. 3 shows.

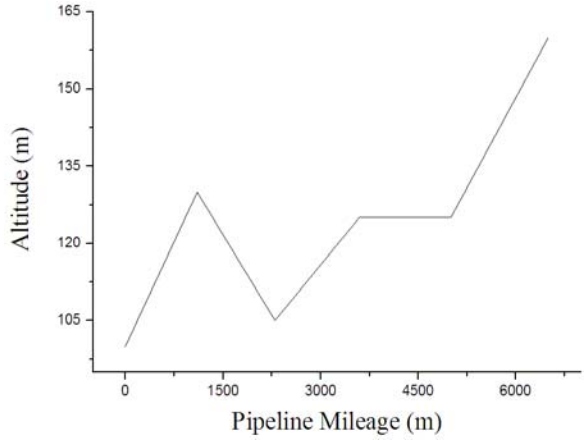

FIG. 2 PIPELINE ROUTE PROFILE

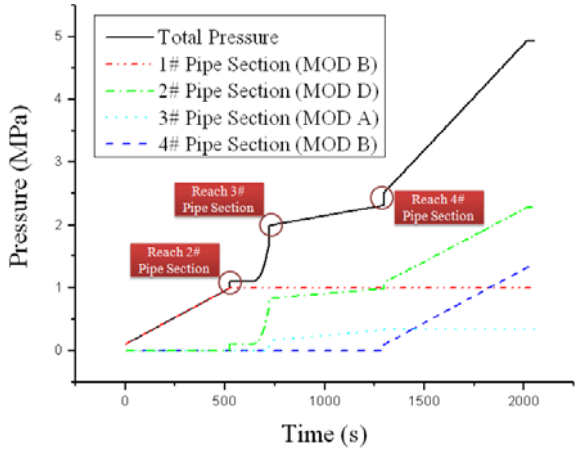

FIG. 3 PRESSURE DROP

It can be seen from Fig. 3 that except for 2# section, the pressure drop of every pipe section only changes when the full pipe flow water front is in it, indicating that its hydraulic status is independent of subsequent sections. As to the 2# section, due to the stagnant air pocket, although full pipe flow water front has passed this section, air pocket still suffers compression, resulting in extra pressure loss, which makes the pressure drop in this pipe section continuously increase. Calculation results show that the extra pressure loss caused by air pocket accounts for about 35% of the total pressure drop of the pipeline.

It can be indicated from the above analysis that the results obtained by this technology are basically reasonable. Meanwhile, with this technology, the calculation time for this simulation example required by ordinary PC is 310 s, which satisfies the engineering requirement.

Summary

This paper develops a novel technology to simulate the pipeline commissioning process. Several alternative modules are established, focused on which physical and mathematical models are established respectively to describe its flow status and corresponding pressure drop. With recognition technology, actual pipeline is divided into several pipe sections matching the corresponding alternative modules. Regulation and control technology are further used to perform the connection of these pipe sections to represent the actual pipeline and thus realizing the simulation of pipeline commissioning process.

ACKNOWLEDGMENT

The study is supported by the National Science Foundation of China (Nos. 51134006, 51176204 and 51276198).

REFERENCES

Boyi Liang. "Study on Hydraulic Characteristics of Oil Pipelines in Commissioning", PhD diss., China University of Petroleum(Beijing), 2011.

C.W. Hirt. "Volume of Fluid(VOF) Method for the Dynamics of Free Boundaries", Journal of Computational Physics, 1981, 39: 201-225.

Guotai Shao. "Commisssioning of Xinggang – Dalian Petrochem Pipeline and Problems to be Focused on", Oil & Gas Storage & Transportation, 2005, 24(12): 61-64.

Jing Gong. "Analysis of Flow Characteristics for Slack Line Flow in a Long Slope Pipeline", Journal of the University of Petroleum, China, 1995, 19(6): 65-72.

Nan Zhang. "Study of the Two Phase Flow in Hilly Pipeline Commissioning", PhD diss., China University of Petroleum(Beijing), 2009.

Nan Zhang. "The Influence of Elevation on the Commissioning of China West Products Pipeline", Oil & Gas Storage & Transportation, 2008, 27(1): 5-8.

Shaoqing Li. "The Commissioning Technology Adopted in Jing' an – Xianyang Oil Pipeline", Oil & Gas Storage & Transportation, 2002, 21(5): 28-29.

Zengqiang Zhang. "Commissioning Technique of Lanzhou – Chengdu – Chongqing Products Pipeline", Oil & Gas Storage & Transportation, 2004, 23(6): 32-35.